

EXPERIMENTAL VALIDATION OF THE RADIANT  
TIME SERIES METHOD FOR COOLING LOAD  
CALCULATIONS

By

IP SENG IU

Bachelor of Science

University of Macau


Taipa, Macau

1999

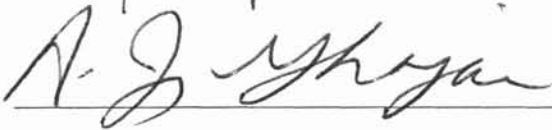
Submitted to the Faculty of the  
Graduate College of the  
Oklahoma State University  
in partial fulfillment of  
the requirements for  
the Degree of  
MASTER OF SCIENCE  
December 2002


EXPERIMENTAL VALIDATION OF THE RADIANT  
TIME SERIES METHOD FOR COOLING LOAD  
CALCULATIONS

Thesis Approved:

  
\_\_\_\_\_  
Thesis Advisor

  
\_\_\_\_\_

  
\_\_\_\_\_

  
\_\_\_\_\_  
Dean of the Graduate College

## ACKNOWLEDGMENTS

I would like to give my sincere appreciation to my major advisor, Dr. Daniel Fisher for his guidance, supervision, financial support and laborious work on this thesis. My appreciation extends to other professors in the OSU HVAC research group, Dr. Jeffery Spitler and Dr. Simon Rees who provided suggestions and assistance for this study.

I wish to express my special appreciation to Dr. Afshin Ghajar for his kindness and advice; Dr. Lap Mou Tam, an OSU alumnus, for his encouragement on my graduate study. Dr Tam's positive attitude towards students and enthusiastic teaching style initiated my study in OSU.

I would like to thank my family and friends for their support and encouragement at times of difficulties. Thanks also go to the project sponsor, ASHRAE for the two years of support.

## TABLE OF CONTENTS

Chapter		Page
1	OVERVIEW OF THE RADIANT TIME SERIES METHOD	1
	1.1 Background -----	1
	1.2 Overview -----	3
2	CALCULATING CONDUCTION TRANSFER FUNCTIONS AND PERIODIC RESPONSE FACTORS FOR COOLING LOAD PROCEDURES	9
	2.1 Introduction -----	9
	2.2 Overview of the Toolkit Conduction Heat Transfer Calculation Procedures -----	11
	2.2.1 The Toolkit Conduction Transfer Function (CTF) Procedure -----	11
	2.2.2 The Toolkit Periodic Response Factor (PRF) Procedure -----	17
	2.3 Using the Toolkit Modules to Calculate CTFs and PRFs -----	21
	2.3.1 Overview of the algorithm -----	21
	2.3.2 Structure of the Algorithm -----	22
	2.4 The Toolkit User Interface to CTF and PRF generator -----	25
	2.5 Evaluation of the Program Outputs -----	27
	2.5.1 Consistency of PRFs and CTFs -----	28
	2.5.2 Comparison with Published Data -----	28
	2.5.3 Steady State Evaluation -----	29
	2.6 Uncertainty Analysis of Conduction to Cooling Load Calculation -----	31
	2.7 Summary and Conclusions -----	34



Chapter		Page
3	BOUNDING THE RANGE OF APPLICABILITY OF CONDUCTION TRANSFER FUNCTION METHODS IN COOLING LOAD AND ENERGY CALCULATIONS	36
3.1	Introduction -----	36
3.2	Overview of the Solution Methods -----	36
3.2.1	Laplace Transform Method -----	37
3.2.2	State-space Method -----	39
3.2.3	Analytical Method -----	40
3.3	Types and Sources of Errors in CTF Solution -----	42
3.3.1	Sources of Errors in CTF Calculation -----	42
3.3.2	Sources of Errors in CTF Application -----	43
3.4	The Test Procedure -----	44
3.5	Results and Discussions -----	47
3.5.1	Single-layered Slabs -----	48
3.5.2	Multi-layered Slabs -----	51
3.6	Conclusions -----	54
4	CALCULATING RADIANT TIME FACTORS FOR THE RADIANT TIME SERIES METHOD PROCEDURES	55
4.1	Introduction -----	55
4.2	Using the Heat Balance Method to Calculate Radiant Time Factors -----	57
4.3	The Interface to the RTF Generator -----	58
4.4	Evaluation of the Program Output -----	60
4.5	Using RTFs in the RTSM -----	63
4.6	Conclusions -----	64
5	EXPERIMENTAL VERIFICATION OF THE RADIANT TIME SERIES METHOD FOR COOLING LOAD CALCULATIONS	65
5.1	Introduction -----	65

Chapter	Page
5.2	Validation Approach ----- 68
5.2.1	Facility Construction and Instrumentation ----- 68
5.2.2	Validation Models ----- 70
5.2.3	Experimental Procedure ----- 74
5.2.4	Experimental Uncertainty ----- 75
5.3	Results and Discussions ----- 77
5.3.1	Predicted Heat Gains ----- 77
5.3.2	Modeling of Thermal Mass Effect ----- 79
5.3.3	Prediction of Peak Cooling Loads ----- 82
5.3.3.1	Test 1: Base Configuration ----- 83
5.3.3.2	Test 2: Suspended Ceiling ----- 84
5.3.3.3	Test 3: Venetian blinds ----- 85
5.3.3.4	Test 4: Carpet ----- 86
5.3.3.5	Test 5: Thermal Mass ----- 87
5.3.3.6	Test 6: Combined Configuration ----- 88
5.3.3.7	Summary of Results ----- 89
5.4	Conclusions and Recommendations ----- 91
6	CONCLUSIONS AND RECOMMENDATIONS 93
6.1	Conclusions ----- 93
6.2	Recommendations ----- 96
	REFERENCES 98

## LIST OF TABLES

Table		Page
1.1	Recommend fixed fractions for radiative and convective heat gain splits.	5
2.1	Calculated conduction transfer functions for Roof 10 by different methods.	15
2.2	Calculated conduction transfer functions for Wall 17 by different methods.	15
2.3	Periodic response factors of Roof 10 ( $\text{W/m}^2\text{-K}$ ).	20
2.4	Periodic response factors of Wall 17 ( $\text{W/m}^2\text{-K}$ ).	20
2.5	Required data values in the toolkit input file for CTF and PRF calculation.	24
2.6	Influence coefficients of overall U-value to total cooling loads.	32
3.1	Default Toolkit settings for CTF solution.	45
4.1	Summations of 24-hour RTFs.	61
5.1	Summary of input parameters and heat transfer models for the RTSM validation.	73
5.2	Comparison of interior convection models.	74
5.3	Test cell configurations.	75
5.4	Typical Light Building Heat Gain Splits.	77
5.5	Summary of peak load errors predicted by RTSM.	89
5.6	Heat gain fractions for typical building configurations.	91

## LIST OF FIGURES

Figure		Page
1.1	Calculation procedures for the radiant time series method.	4
2.1	CTF schematic diagram.	13
2.2	Periodic response factors for Roof 10 and Wall 17.	18
2.3	Comparisons of State-space and Laplace PRFs.	21
2.4	CTF and PRF calculation framework.	22
2.5	Structure of the toolkit CTF and PRF calculations.	23
2.6	Dialog box used for creating toolkit input file.	26
2.7	Material database.	27
2.8	Comparisons of U-values.	28
2.9	Comparison of the PRF generator outputs to the PRF database of Spitler et al. (2000)	29
2.10	Comparison of the PRF generator U-values to the steady-state U-values.	30
2.11	Perturbation of PRFs.	32
2.12	The influence of the U-value error to the total cooling load error.	33
3.1	The generation of response factors.	37
3.2	CTF test procedure scheme.	45
3.3	Error measured in the CTF solution test (Arrows indicate error).	47
3.4	Single-layered CTF solution errors.	49
3.5	Maximum errors in the single-layered test.	50

Figure		Page
3.6	CTF solutions error for $1/Fo \approx 44.5$ .	50
3.7	Single-layered CTF solution error (with thermal structure factor).	52
3.8	3-layered CTF solution error.	52
3.9	6-layered CTF solution error.	53
3.10	First values of $1/(FoS_{ie})$ that cause more than 5% error in the CTF solutions.	53
4.1	Radiant Time Factors for different materials and radiant distributions.	56
4.2	The RTF calculation procedures using HBM.	58
4.3	Configure RTF calculations.	59
4.4	The computer program interface to generate RTFs.	60
4.5	RTFs for concrete zones.	62
4.6	RTFs for plywood zones.	62
4.7	RTFs for steel zones.	62
4.8	Insulation board zones.	63
5.1	Opposing Temperature Gradients Predicted by HBM and RTSM.	66
5.2	RTSM Modified to Correct Errors.	67
5.3	Terminal reheat system used in the RTSM validation (not to scale).	69
5.4	Comparison of Toolkit Results with Rees Parametric Study (Rees 2002).	78
5.5	Periodic Response Factors for Test Buildings Surfaces.	79
5.6	Radiant Time Factors for Test Buildings.	80
5.7	Thermal Mass Effects.	81

Figure		Page
5.8	Test 1 - Base configuration.	83
5.9	Test cell configurations.	85
5.10	Test 2 - Suspended ceiling.	85
5.11	Test 3 - Blind with slats at 45°.	86
5.12	Test 4 – Carpet.	87
5.13	Test 5 –Thermal mass.	88
5.14	Test 6 - Combined configuration.	88
5.15	Simulation for typical building configurations.	90

## NOMENCLATURE

### English letter symbols

$a$	Coefficient matrix that depends on material properties, and/or film coefficients
$A(s)$	Overall transmission matrix that depend on material properties, and/or film coefficients.
$b$	Coefficient matrix that depends on material properties, and/or film coefficients
$b$	24×24 air-to-air cross CTF coefficient matrix
$b_n$	Air-to-air cross CTF coefficient, $W/(m^2-K)$ or $Btu/(hr-ft^2-F)$
$B(s)$	Overall transmission matrix that depend on material properties, and/or film coefficients.
$c$	Coefficient matrix that depends on material properties, and/or film coefficients
$c_n$	Air-to-air interior CTF coefficient, $W/(m^2-K)$ or $Btu/(hr-ft^2-F)$
$c_p$	Specific heat, $J/(kg-k)$ or $Btu/(lbm-F)$
$C$	Thermal capacitance, $J/C$ or $Btu/F$
$C_T$	Total thermal capacitance, $J/(m^2-C)$ or $Btu/(ft^2-F)$
$d$	Coefficient matrix that depends on material properties, and/or film coefficients
$d$	24×24 air-to-air flux CTF coefficient matrix
$d_n$	Air-to-air flux CTF coefficient, $W/(m^2-K)$ or $Btu/(hr-ft^2-F)$
$D(s)$	Overall transmission matrix that depend on material properties, and/or film coefficients.

$e_a$	Fraction error in nozzle area
$e_c$	Fraction error in nozzle discharge coefficient
$e_Q$	Fraction error in cooling load
$e_{fs}$	Fraction variation in fan speed
$e_{sp}$	Fraction error in static pressure
$e_{\Delta p}$	Fraction error in pressure drop across flow nozzles
$e_{\Delta T}$	Uncertainty in temperature difference, C or F
$e_v$	Uncertainty in volumetric flow rate
$E$	CTF solution error
$E_t$	Total solar radiation incident on surface, Btu/(hr-ft <sup>2</sup> -F) or W/(m <sup>2</sup> -C)
$f$	Decrement factor, dimensionless
$f_c$	Convective fraction of conduction heat gain
$f_r$	Radiative fraction of conduction heat gain
$F_g$	Long wave radiant ground view factor
$F_{sky}$	Long wave radiant sky view factor
$Fo$	Fourier number
$h_o$	Coefficient of heat transfer by long-wave radiation and convection at outer surface, Btu/(hr-ft <sup>2</sup> -F) or W/(m <sup>2</sup> -C)
$H_{in}$	Conduction flux history at inside surface, W/(m <sup>2</sup> -K) or Btu/(hr-ft <sup>2</sup> -F)
$H_{out}$	Conduction flux history at outside surface, W/(m <sup>2</sup> -K) or Btu/(hr-ft <sup>2</sup> -F)
$k$	Thermal conductivity, W/(m-C) or (Btu-in)/(hr-ft <sup>2</sup> -F)
$L$	Material layer thickness, m or in
$\dot{m}$	Mass flow rate of air, kg/s or lbm/s



$N_x$	Number of exterior CTF terms
$N_y$	Number of cross CTF terms
$N_z$	Number of interior CTF terms
$N_\phi$	Number of flux CTF terms
$N_{node}$	Number of state-space nodes
$r_n$	Radiant time factors
$R$	Thermal resistance, $(m^2-C)/W$ or $(hr-ft^2-F)/Btu$
$R_c$	Film resistance due to convection, $(ft^2-F-hr)/Btu$ or $(m^2-C)/W$
$R_r$	Film resistance due to radiation, $(ft^2-F-hr)/Btu$ or $(m^2-C)/W$
$R_T$	Total thermal resistance, $(m^2-C)/W$ or $(hr-ft^2-F)/Btu$
$R_{i-m}$	Resistance from the surface of layer m to inner surroundings, $(m^2-C)/W$ or $(hr-ft^2-F)/Btu$
$R_{m-o}$	Resistance from the surface of layer m to outer surroundings, $(m^2-C)/W$ or $(hr-ft^2-F)/Btu$
$P$	24×24 PRF matrix
$P_n$	Periodic response factors, $W/(m^2-K)$ or $Btu/(hr-ft^2-F)$
$q$	Heat gains, W or Btu/hr
$q_{tot}$	Total heat gain, W or Btu/hr
$q''$	Heat flux, $W/m^2$ or $Btu/(hr-ft^2)$
$q''_e$	Air-to-air conduction heat flux, $W/m^2$ or $Btu/(ft^2-hr)$
$q''_{ki}$	Conduction heat flux at interior surface, $W/m^2$ or $Btu/(hr-ft^2)$
$q''_{ko}$	Conduction heat flux at exterior surface, $W/m^2$ or $Btu/(hr-ft^2)$
$q''_{ki}(s)$	Inside conduction heat flux in Laplace domain
$q''_{ko}(s)$	Outside conduction heat flux in Laplace domain

$q''_{exact}$	Peak conduction heat flux from exact solution, W/m <sup>2</sup> or Btu/(hr-ft <sup>2</sup> )
$q''_{num}$	Value of conduction heat flux from numerical solution at the time the exact peak conduction heat flux is measured, W/m <sup>2</sup> or Btu/(hr-ft <sup>2</sup> )
$q_{diffuse}$	Diffuse solar radiation, W or Btu/hr
$q_{r,beam}$	Reflected diffuse solar radiation from beam solar radiation transmitted
$q_{sw}$	Short wave radiation heat gain, W or Btu/hr from windows, W or Btu/hr
$q_{sw,int}$	Short wave radiation from internal heat gains, W or Btu/hr
$q_{sw,loss}$	Total short wave heat loss from windows, W or Btu/hr
$q^*$	Heat gain fraction
$q^*_{cond}$	Fraction of air-to-air conduction heat gain
$q^*_{infil}$	Fraction of infiltration heat gain
$q^*_{internal}$	Fraction of internal heat gains
$q^*_{solar}$	Fraction of transmitted solar heat gains
$Q$	Cooling/heating load, W or Btu/hr
$Q_N$	Normalized cooling load
$Q_{est}$	Estimated cooling load, W or Btu/hr
$Q_{max,exp}$	Maximum measured cooling load, W or Btu/hr
$Q_{min,exp}$	Minimum measured cooling load, W or Btu/hr
$s$	Surface solar fraction that represents the portion of solar heat gain on surface
$s_{floor}$	Solar fraction of floor
$S_{ie}$	Thermal structure factor, dimensionless
$t$	Time, sec
$T$	Temperature, C or F

$T_A$	Amplitude of the sinusoidal temperature variation, C or F
$T_e$	Sol-air temperature, C or F
$T_g$	Ground surface temperature, F or C
$T_i$	Interior boundary temperature, C or F
$T_m$	Mean air temperature of the sinusoidal temperature variation, C or F
$T_o$	Exterior boundary temperature, C or F
$T_{is}$	Interior surface temperature, C or F
$T_{os}$	Exterior surface temperature, C or F
$T_{in}$	Test cell inlet air temperature, C or F
$T_{out}$	Test cell outlet air temperature, C or F
$T_{rc}$	Constant room air temperature, C or F
$T_{sky}$	Sky temperature, F or C
$T_i(s)$	Interior boundary temperature in Laplace domain
$T_o(s)$	Exterior boundary temperature in Laplace domain
$U$	Overall heat transfer coefficient, W/(m <sup>2</sup> -K) or Btu/(hr-ft <sup>2</sup> -F)
$U_f$	Air-to-air overall heat transfer coefficient, W/(m <sup>2</sup> -K) or Btu/(hr-ft <sup>2</sup> -F)
$x$	Heat flow direction, m or ft
$X_n$	Surface-to-surface exterior CTF coefficient, W/(m <sup>2</sup> -K) or Btu/(hr-ft <sup>2</sup> -F)
$Y_n$	Surface-to-surface cross CTF coefficient, W/(m <sup>2</sup> -K) or Btu/(hr-ft <sup>2</sup> -F)
$Z_n$	Surface-to-surface interior CTF coefficient, W/(m <sup>2</sup> -K) or Btu/(hr-ft <sup>2</sup> -F)
$\Delta T$	Temperature difference, C or F

### Greek letter symbols

$\alpha$	Thermal diffusivity, m <sup>2</sup> /s or ft <sup>2</sup> /s
$\alpha_s$	Absorptance of surface for solar radiation
$\delta$	Time step, hour
$\varepsilon$	Hemispherical emittance of surface
$\theta$	Current hour
$\rho$	Material density, kg/m <sup>3</sup> or lbm/ft <sup>3</sup>
$\rho_{t, floor}$	Floor surface short wave reflectance
$\sigma$	Stefan-Boltzmann constant, 5.67E-8 W/(m <sup>2</sup> -K <sup>4</sup> ) or 1.17E-9 Btu/(hr-ft <sup>2</sup> -F <sup>4</sup> )
$\tau_i$	Window diffuse transmittance
$\phi$	Time lag, hour
$\phi_n$	Surface-to-surface flux CTF coefficient
$\dot{v}$	Measured volumetric flow rate, m <sup>3</sup> /s or ft <sup>3</sup> /s
$\omega$	Frequency of the sinusoidal temperature function

## CHAPTER 1

### OVERVIEW OF THE RADIANT TIME SERIES METHOD

#### 1.1 Background

Cooling load calculation methods have been developing and improving for decades. From the Total Equivalent Temperature Difference/Time Averaging (TETD/TA) method (ASHRAE, 1967), U.K.'s Admittance Method (Loudon 1968), Transfer Function method (TFM) (ASHRAE, 1972), and Cooling Load Temperature Difference/Solar Cooling Load/Cooling Load Factor (CLTD/SCL/CLF) method (ASHRAE, 1977), to the most recent Heat Balance method (HBM) (Pedersen et al. 1997) and Radiant Time Series Method (RTSM) (Spitler et al. 1997), all of them can be used in estimating cooling load for a designed building space. The HBM is considered the most fundamental and general of all because it explicitly models the heat transfer rates to the interior and exterior surfaces, and the zone air. It is the standard ASHRAE load calculation method as described in the ASHRAE handbook of fundamentals (2001). This method is based on simultaneously satisfying a system of equations that includes a zone air heat balance and a set of outside and inside heat balances at each surface/air interface. The system of equations may be solved in a computer program using successive substitution, Newton techniques or (with linearized radiation) matrix methods. The only disadvantage of the HBM is that it requires detailed input and a computer implementation to solve the hourly simultaneous heat balance equations.

The other recently developed cooling load calculation method, the RTSM is a simplified cooling load calculation method documented in the 2001 ASHRAE handbook-fundamentals. It has replaced the TETD/TA, CLTD/SCL/CLF and TFM methods that are described in earlier editions of the handbook. RTSM is a simplified method that does not solve the heat balance equations. The method is “heat-balance based” to the extent that the storage and release of energy in the zone is approximated by a set of predetermined zone response factors, called radiant time factors (RTFs) (Spitler et al. 1997). The transient conduction calculation is approximated using another set of predetermined thermal response factors, called periodic response factors (PRFs), which relate conduction heat gains directly to temperatures only. By incorporating these simplifications, the RTSM calculation procedure becomes explicit, avoiding the requirement to solve the simultaneous system of heat balance equations. The RTSM shares many of the heat transfer sub-models used by the HBM and has the equivalent principle of superposition used in the TFM (Spitler et al. 1999). Moreover, it is a rather simplified method that does not require iterative calculations like the HBM and the TFM. If the radiant time factors (RTFs) and the periodic response factors (PRFs) for a particular zone configuration are known, the RTSM may be implemented in a spreadsheet. The method is useful not only for peak load calculations, but also for estimating component contributions to the hourly cooling loads that is useful for both pedagogy and design.

Immediately following development of the RTSM, the new method was verified by comparing cooling loads predicted by the RTSM with cooling loads predicted by the heat balance for a wide range of zone configurations. Rees, et al (1998) compared RTSM and heat balance cooling loads for 1296 configurations, which were generated by

parametrically varying significant input parameters over a wide range. This analysis conclusively demonstrated that the RTSM always produces a conservative estimate of the cooling load when compared to the heat balance method. However, the over-prediction of the cooling load by the RTSM tends to increase as the fraction of window area in the zone increases. Since the HBM and RTSM share most of the heat transfer models in the cooling load calculation, the PRF and RTF models that are used exclusively in the RTSM are considered the most likely sources of error. This thesis first investigates the applicability and validity of using PRFs in conduction calculations. PRFs were compared to previously published values and validated using both steady state and transient tests. Second, the calculation of RTFs is presented. The validity of using RTFs in cooling load calculation is validated experimentally to justify the approximation of energy storage and release in the RTSM. Finally, the overall RTSM performance is discussed and analyzed based on the experimental results and the RTSM calculation procedures. Implementation and improvement of the RTSM procedures are also addressed.

## **1.2 Overview**

The RTSM calculation procedure is illustrated in figure 1.1 (Spitler et al. 1997).

The procedures can be summarized as follows:

1. Calculate hourly internal heat gains.
2. Calculate hourly conduction heat gains for each surface using PRFs.
3. Calculate hourly beam and diffuse transmitted, and absorbed solar heat gains through glazed surfaces.
4. Split all heat gains into convective and radiative portions.

5. Determine hourly infiltration heat gains.
6. Sum hourly the convective portion of the heat gain with the infiltration heat gain.
7. Convert radiant heat gains into hourly cooling loads using RTFs. The beam RTFs operate on the portion of the radiant heat gains that is distributed and absorbed by the floor. The diffuse RTFs operate on the other portion of the radiant heat gains that is uniformly distributed to the zone interior surfaces.
8. Sum the resulting hourly convective heat gains from step 6 with the converted hourly cooling loads from steps 7. The result is the hourly cooling load.

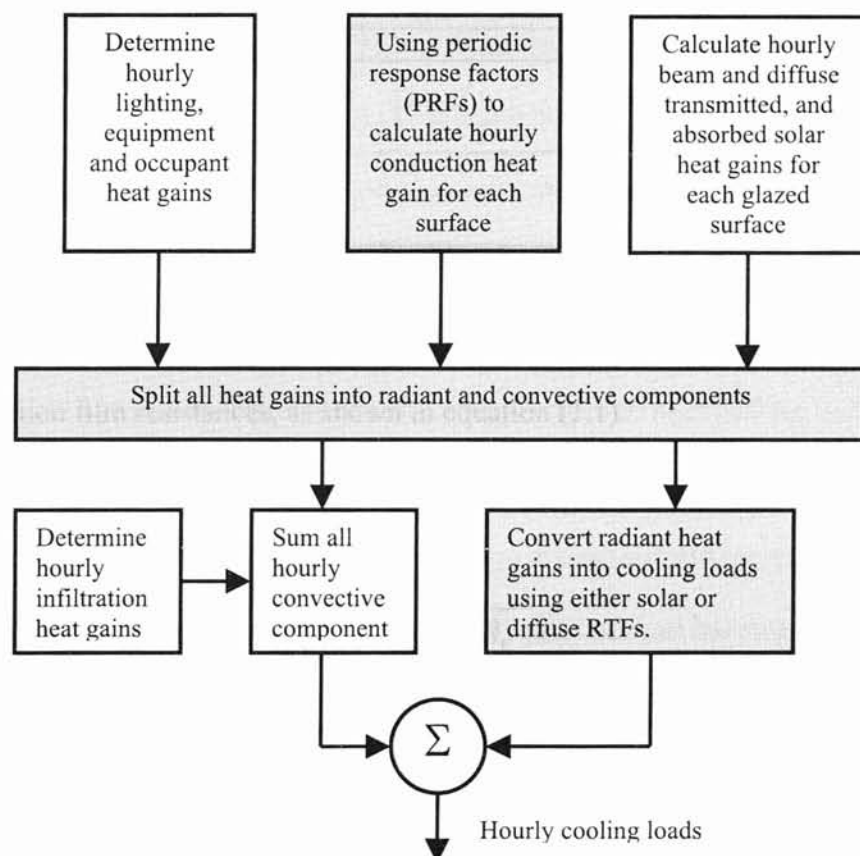


**Figure 1.1 Calculation procedures for the radiant time series method.**

The heat gain split in the RTSM simplifies the calculation of radiation exchange between interior surfaces. The radiation exchange is dependent on the surface temperatures and



emissivities, so in general, it is solved simultaneously with the convection heat transfer. An iteration procedure is typically applied to solve this problem. The RTSM decouples these two heat transfer processes by splitting heat gains into radiative and convective portions using some fixed fractions. The recommended fixed fractions are listed in table 1.1 (Spitler et al. 1997).

**Table 1.1 Recommend fixed fractions for radiative and convective heat gain splits.**

Heat Gain Type	Radiative	Convective
Occupants	0.7	0.3
Lighting:		
Suspended fluorescent-unvented	0.67	0.33
Recessed fluorescent-vented to return air	0.59	0.41
Recessed fluorescent-vented to supply and return air	0.19	0.81
Incandescent	0.71	0.29
Equipment	0.2-0.8	0.8-0.2
Conduction heat gain:		
Walls	0.63	0.37
Roofs	0.84	0.16
Solar Radiation:		
Transmitted	1	0
Absorbed (by fenestration)	0.63	0.37

Conduction heat gains can be split according to the relative magnitude of the radiation and convection film resistances, as shown in equation (1.1).

$$f_c = 1 - f_r \quad (1.1b)$$

$$f_r = \frac{R_c}{R_r + R_c} \quad (1.1a)$$

After the heat gains are split, the convective portion is the direct contribution to the instantaneous cooling load, while the radiative portion is absorbed by the building elements, and then convected back to the zone air to become cooling load. The conversion from radiative heat gains to cooling loads requires the use of RTFs.

The calculations in the shaded boxes shown in figure 1.1 represent the major differences between the RTSM and the TFM that primarily eliminate the necessity of iteration in the other method. As a result, the computational procedures of the RTSM are simple and straightforward.

While the calculation is simple, the following assumptions apply to the RTSM (McQuiston et al. 2000):

- All external and internal driving forces are steady-periodic. In addition, the zone air temperature is assumed to be constant.
- All surface heat gains are eventually converted to cooling loads. In other words, no portion of a surface heat gain can be lost from the space at a later time. This is the so-called ‘adiabatic zone’ assumption. This assumption is essential in the generation of RTFs, which represents the response of an adiabatic zone to a unit radiant pulse.
- PRFs and RTFs are predetermined coefficients.
- Solar transmitted beam radiation is distributed on the floor only, while other short wave and long wave radiation is distributed uniformly on each surface in the building space.
- The outside and inside heat transfer coefficients are time-invariant and are the combined effect of convection and radiation. Unlike the heat balance method (Pedersen et al. 1997), RTSM does not have detailed surface and air heat balance models, instead, outside radiation and convection are modeled together with an equivalent temperature, called the sol-air temperature which operates on the “air-to-air” periodic response factors (PRFs). The sol-air temperature is calculated as:

$$T_{e,\theta} = T_{o,\theta} + \frac{\alpha_s E_{t,\theta}}{h_{o,\theta}} + \frac{\varepsilon\sigma}{h_{o,\theta}} \left[ F_{sky} (T_{sky,\theta}^4 - T_{o,\theta}^4) + F_g (T_g^4 - T_o^4) \right] \quad (1.2)$$

A simplified expression of equation (3) is presented in the ASHRAE Handbook of Fundamentals (ASHRAE, 2001) as:

$$T_{e,\theta} = T_{o,\theta} + \frac{\alpha_s E_{t,\theta}}{h_{o,\theta}} - \frac{\varepsilon\Delta R}{h_{o,\theta}} \quad (1.3)$$

The term  $\frac{\varepsilon\Delta R}{h_{o,\theta}}$  is called the long-wave correction, which is about 3.9 C or 7.02 F for

horizontal surfaces and zero for vertical surfaces. Moreover, it is usually assumed that  $h_o = 17 \text{ W}/(\text{m}^2\text{-C})$  or  $2.99 \text{ Btu}/(\text{hr-ft}^2\text{-F})$ .

As shown in figure 1.1, PRFs are used in the conduction calculation in the RTSM. PRFs represent the transient conduction response of each surface on a building envelope with the combined effects of convection and radiation on the inside and outside surfaces. The use of PRFs and the accuracy of the PRFs themselves are therefore important to the overall cooling load calculation. Detailed discussions of PRFs are addressed in the next two chapters. Chapter 2 discusses the calculation and application of PRFs, where the relationship between conduction transfer functions (CTFs) and PRFs are presented. Chapter 3 discusses the accuracy of CTFs and their consequent influence on conduction calculations in the RTSM.

While PRFs represent the thermal response of a surface construction, RTFs represent the thermal response of a zone and account for the time lag and dampening effects of radiative heat gains. As shown in figure 1.1, the use of RTFs in the RTSM converts the radiant heat gains to approximate the instantaneous cooling loads, and eliminates the need to solve the system of zone air and surface heat balance equations.

Since different types of radiant heat gains are assumed to be distributed differently, two separate series of radiant time factors (beam and diffuse) are required to accomplish the cooling load conversions. The physical significance and the intrinsic assumptions of the RTFs are therefore influential in the overall cooling load calculation. A detailed calculation of RTFs is presented in chapter 4. An experimental validation of the use of RTFs in cooling load calculations is addressed in chapter 5, where its influence on the overall cooling load calculation is discussed.

A detailed explanation of the RTSM can be found in the ASHRAE Loads Toolkit (2001). The ASHRAE Loads Toolkit is the ASHRAE standard for cooling load calculations; it contains well-documented heat transfer models in modular format. Toolkit users can write a simple driver subroutine to use individual modules, or develop a heat balance based cooling load application. The Toolkit therefore provides a convenient computational and analytical platform for validating the RTSM.

## CHAPTER 2

# CALCULATING CONDUCTION TRANSFER FUNCTIONS AND PERIODIC RESPONSE FACTORS FOR COOLING LOAD PROCEDURES

### 2.1 Introduction

In order to effectively use the ASHRAE cooling load calculation procedures, it is necessary to understand and correctly apply both the periodic response factors (PRFs) in the RTSM and the conduction transfer functions (CTFs) in the HBM. The PRFs and CTFs are closely related to each other and both represent the transient thermal response of a surface construction. Although response factor and transfer function methods are well established in the literature (Stephenson and Mitalas, 1971; Hittle, 1979; Ceylan and Myers, 1980; Seem, 1987; Ouyang and Haghghat, 1991), misconceptions persist concerning their application to cooling load procedures. Several forms of the equations relating to different boundary conditions are found in the literature. Methods of calculating the coefficients differ, and their accuracy is not easily checked. The objective of this chapter is to reconcile the various forms of the transfer function equations, discuss implicit assumptions associated with each form and illustrate by way of an example calculation the use of the various methods. Particular attention is given to the conduction transfer function methods presented in the ASHRAE Loads Toolkit. An algorithm that uses the Toolkit CTF module is presented along with a simple program to generate CTFs and PRFs for use in cooling load procedures.

In both the HBM and the RTSM, two simplifying assumptions are made in solving the wall heat conduction problem. First, heat conduction is assumed to be one-dimensional. Two-dimensional effects due to corners and non-uniform boundary conditions are neglected. Second, materials are assumed to be homogeneous and have constant thermal properties. Although the one-dimensional, transient conduction problem can be solved analytically, the analytical solution is immediately complicated when the analysis is extended to multi-layered constructions. Analytical solutions for multi-layered slabs require special mathematic functions and complex algebra. Ultimately, numerical methods must be employed at some level to solve the problem. Solution techniques include lumped parameter methods, frequency response methods, finite difference or finite element methods, and Z-transform methods (McQuiston, et al. 2000). The Toolkit implements Laplace and state-space methods for calculating CTFs and provides an algorithm to derive PRFs from a set of CTFs.

CTFs and PRFs are dependent only on material properties and reflect the transient response of a given construction for any set of environmental boundary conditions. Since material properties are typically assumed to be constant in HVAC thermal load calculations, it is possible to pre-calculate these coefficients. Although CTFs and PRFs for typical constructions are available in the ASHRAE handbook of fundamentals (1997) and Spitler, et al. (2000), respectively, the ASHRAE Loads Toolkit (Pedersen, 2001) makes it possible to quickly and accurately construct a stand-alone computer program that will calculate CTFs and PRFs for any arbitrary wall configuration. This chapter presents an algorithm for pre-calculating these coefficients using the Toolkit modules.

## 2.2 Overview of the Toolkit Conduction Heat Transfer Calculation Procedures

The Toolkit conduction algorithms pre-calculate the coefficients that are used in the heat balance based methods. The HBM uses CTFs, while the RTSM uses PRFs. In the HBM, the instantaneous conduction flux is represented by a simple linear equation that relates the current rate of conduction heat transfer to temperature and flux histories, while in RTSM, the conduction flux is a linear function of temperatures only.

### 2.2.1 The Toolkit Conduction Transfer Function (CTF) Procedure

In cooling load and energy calculations, conduction heat transfer is usually modeled as a 1-dimensional, transient process with constant material properties (McQuiston, et al. 2000). The simplified heat diffusion equation in Cartesian coordinates is shown in equation (2.1) (Incropera, et al. 1996).

$$\frac{\partial^2 T(x,t)}{\partial x^2} = \frac{1}{\alpha} \frac{\partial T(x,t)}{\partial t} \quad (2.1)$$

Fourier's law, equation (2.2), specifies the conduction heat flux in terms of the thermal conductivity of the material and temperature gradient across a differential thickness.

$$q'' = -k \frac{\partial T(x,t)}{\partial x} \quad (2.2)$$

Since equation (2.1) is a partial differential equation, the system is usually solved numerically, often by means of conduction transfer function (CTF) methods. CTFs represent the material's thermal response as determined by its material properties. The method results in a simple linear equation that expresses the current heat flux in terms of the current temperature, and temperature and heat flux histories. The linear form of

equations (2.3) and (2.4) greatly reduce the required computational effort compared to other numerical techniques and facilitates computer implementation of the CTF method.

The CTF formulation of the surface heat fluxes involves four sets of coefficients. Following Spitler's nomenclature (McQuiston, et al. 2000)  $X$ ,  $Z$ , and  $Y$  are used to represent the exterior, interior and cross terms respectively. Equation (2.3) shows the zeroth outside and cross terms operating on the current hour's surface temperatures.  $H_{out}$  is the flux history term as shown in (2.3a). Together the current hour's surface temperatures and the history term yield the total flux at the outside surface.

$$q_{ko,\theta}'' = -Y_0 T_{is,\theta} + X_0 T_{os,\theta} + H_{out} \quad (2.3)$$

$$\text{where: } H_{out} = -\sum_{n=1}^{N_y} Y_n T_{is,\theta-n\delta} + \sum_{n=1}^{N_x} X_n T_{os,\theta-n\delta} + \sum_{n=1}^{N_\phi} \phi_n q_{ko,\theta-n\delta}'' \quad (2.3a)$$

Likewise, equations (2.4) and (2.4a) show the flux at the inside surface.

$$q_{ki,\theta}'' = -Z_0 T_{is,\theta} + Y_0 T_{os,\theta} + H_{in} \quad (2.4)$$

$$\text{where: } H_{in} = -\sum_{n=1}^{N_z} Z_n T_{is,\theta-n\delta} + \sum_{n=1}^{N_y} Y_n T_{os,\theta-n\delta} + \sum_{n=1}^{N_\phi} \phi_n q_{ki,\theta-n\delta}'' \quad (2.4a)$$

As indicated in equations (2.3) and (2.4), the current heat fluxes are closely related to the flux histories. The flux histories, shown as constant terms in equations (2.3) and (2.4), are not only related to previous surface temperatures, but are also related to previous heat fluxes. Equations (2.3) and (2.3a) or equations (2.4) and (2.4a) are usually solved iteratively with an assumption that all previous heat fluxes are equal at the beginning of the iteration. The converged solution produces flux history terms ( $H_{out}$  and  $H_{in}$ ) that account for the thermal capacitance of a given construction.



The temperatures operated on by the transfer functions may be either surface or air temperatures. “Surface-to-surface” CTFs, which operate on surface temperatures and are required by the heat balance method, have the advantage of allowing for variable convective heat transfer coefficients. “Air-to-air” CTFs operate between either the sol-air temperature or the air temperature on the outside and the air setpoint temperature on the inside. Air-to-air CTFs include the appropriate film coefficients as resistive layers in the wall assembly. As shown in figure 2.1, surface-to-surface CTFs are represented by the thermal circuit between  $T_{os}$  and  $T_{is}$ , while air-to-air CTS are represented by the thermal circuit between  $T_o$  and  $T_i$ . For constructions with the same material layer arrangement and properties, the surface-to-surface CTFs are always the same, while air-to-air CTFs differ depending on the selected values of the film coefficients.

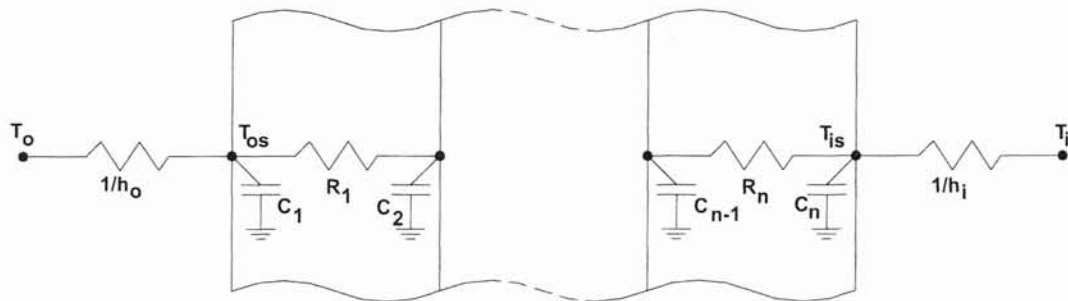


**Figure 2.1 CTF schematic diagram.**

The ASHRAE handbook of fundamentals (1997) presents an “air-to-air” conduction equation that includes additional simplifications. The  $b$  and  $c$  terms shown in equation (2.5) operate on the sol-air temperature and the constant room air temperature respectively.

$$q_{e,\theta}'' = \sum_{n=0}^6 b_n T_{e,\theta-n\delta}'' - \sum_{n=1}^6 d_n q_{e,\theta-n\delta}'' - T_{rc} \sum_{n=0}^6 c_n \quad (2.5)$$

It should be noted that equation (2.5) is suitable only for load calculations. Historically, it was used in the Transfer Function Method (TFM) (McQuiston, 1992) and can be used without loss of generality in the RTSM.

Although equations (2.3) through (2.5) are solutions to the transient, one dimensional conduction problem, it is useful to consider the steady-state limit of these equations. Under steady state conditions, the exterior and interior heat fluxes are equal and the following identities are readily apparent:

$$\sum_{n=0}^{N_x} X_n = \sum_{n=0}^{N_y} Y_n = \sum_{n=0}^{N_z} Z_n \quad \text{or} \quad \sum_{n=0}^6 b_n = \sum_{n=0}^6 c_n \quad (2.6)$$

In combination with the standard formulation for steady state heat transfer through a wall ( $q'' = U\Delta T$ ) an expression for  $U$ , the overall heat transfer coefficient, in terms of conduction transfer functions can be derived as shown in equation (2.7).

$$U = \frac{\sum_{n=0}^{N_y} Y_n}{1 - \sum_{n=1}^{N_\phi} \phi_n} \quad \text{or} \quad U_f = \frac{\sum_{n=0}^6 b_n}{\sum_{n=1}^6 d_n} \quad (2.7)$$

The Toolkit presents two widely used CTF calculation methods. These are the state space method (Ceylan and Myers, 1980; Seem, 1987; Ouyang and Haghghat, 1991) and the Laplace method (Stephenson and Mitalas, 1971; Hittle, 1979). These methods are discussed in greater detail in chapter 3. Tables 2.1 and 2.2 list the sample CTFs from the state-space and the Laplace methods for the ASHRAE roof 10 and wall 17, respectively (ASHRAE, 2001).

**Table 2.1 Calculated conduction transfer functions for Roof 10 by different methods.**

Method	State-space			Laplace		
	CTFs	$b_n W/(m^2-K)$	$c_n W/(m^2-K)$	$d_n$	$b_n W/(m^2-K)$	$c_n W/(m^2-K)$
0	1.843414E-02	1.558694	--	1.792318E-02	1.557600	--
1	1.527098E-01	-1.533850	3.918097E-01	1.526971E-01	-1.529852	3.900831E-01
2	6.914318E-02	2.240878E-01	-3.009094E-02	7.002752E-02	2.213133E-01	-2.952877E-02
3	2.162486E-03	-6.483956E-03	3.063750E-05	2.253625E-03	-6.154021E-03	--
4	1.980676E-06	4.434842E-06	-1.077005E-09	--	--	--
5	3.625569E-11	-6.003775E-11	2.347952E-15	--	--	--
Sum	2.424516E-01	2.424515E-01	3.617494E-01	2.429014E-01	2.429075E-01	3.605544E-01
U-values W/(m <sup>2</sup> -K)	3.798689E-01			3.798625E-01		

**Table 2.2 Calculated conduction transfer functions for Wall 17 by different methods.**

Method	State-space			Laplace		
	CTFs	$b_n W/(m^2-K)$	$c_n W/(m^2-K)$	$d_n$	$b_n W/(m^2-K)$	$c_n W/(m^2-K)$
0	2.869363E-05	6.280103E+00	--	2.211386E-05	6.245883E+00	--
1	3.423279E-03	-1.206734E+01	1.718700E+00	3.286662E-03	-1.192994E+01	1.711293E+00
2	1.402296E-02	6.833955E+00	-8.513353E-01	1.424779E-02	6.666098E+00	-8.389864E-01
3	8.060353E-03	-1.064722E+00	9.941873E-02	8.194158E-03	-9.936960E-01	9.386551E-02
4	7.410495E-04	4.456763E-02	-3.189737E-03	7.122383E-04	3.828839E-02	-2.832696E-03
5	8.310480E-06	-2.746161E-04	2.084494E-06	6.732527E-06	-1.645613E-04	--
6	6.751854E-09	9.757261E-08	-3.052842E-10	--	--	--
7	2.930320E-13	-8.572414E-12	1.456093E-16	--	--	--
Sum	2.628465E-02	2.628500E-02	9.635963E-01	2.646970E-02	2.647005E-02	9.633400E-01
U-values W/(m <sup>2</sup> -K)	7.220317E-01			7.220321E-01		

The descriptions of these constructions are as follows.

Roof 10 – An eight-layer construction consisting membrane, sheathing, insulation board, metal deck, suspended acoustical ceiling.

Wall 17 – A six-layer construction consisting brick, insulation board and brick.

Note that as presented in the handbook, the inside and outside layers of these construction types are resistance layers that model the combined effects of radiation and convection on inside and outside surfaces respectively; the resulting CTFs are therefore air-to-air type. The data on the right hand side of the tables are calculated from the Laplace method, while the data on the left hand side are from the state space method. The summation of each CTF series and the U-values are also shown in the tables for comparison. Note that conduction transfer functions are not unique for any construction. The differences can be in terms of the number of CTF terms, and/or numerical values. However, under steady state condition, CTFs calculated by various methods will predict the same U-value. As shown in table 2.1, CTFs from both the state space and Laplace methods predict nearly the same overall heat transfer coefficient. Discussions comparing CTF calculation methods can be found in the literature (Ouyang and Haghghat, 1991; Celyan and Myers, 1980).

The number of CTF terms generated by the Toolkit algorithms is determined by the thermal mass of the construction materials. The more thermally massive wall 17 has eight CTF terms, while the relatively lightweight Roof 10 has six. The more thermally massive the construction, the greater the number of CTF terms regardless of the CTF solution technique used. Although the maximum number of terms reported in the ASHRAE handbook of fundamentals is seven, thermally massive constructions may require more terms for accurate calculations (Giaconia and Orioli, 2000). The Toolkit algorithms address this problem by automatically selecting an appropriate number of CTF terms. The maximum number of CTF terms is limited to 19 in the Toolkit.

### 2.2.2 The Toolkit Periodic Response Factor (PRF) Procedure

As formulated in the Toolkit, the RTSM for design load calculations uses periodic response factors rather than CTFs to calculate conduction heat transfer through walls and roofs. As shown in equation (2.8), PRFs operate only on temperatures; the current surface heat flux is a function only of temperatures and does not rely on previous heat fluxes.

$$q_{\theta}'' = \sum_{j=0}^{23} P_j (T_{e,\theta-j\delta} - T_{rc}) \quad (2.8)$$

Equation (2.8) is premised on the steady, periodic nature of the sol-air temperature over a 24-hour period (Spitler et al. 1997). Although the number of PRFs may vary, the twenty-four PRFs shown in equation (2.8) correspond to 24 hourly changes in the sol-air temperature for a single diurnal cycle. It is clear from equation (2.8) that the overall heat transfer coefficient,  $U$ , is represented by the sum of the periodic response factors as shown in equation (2.9).

$$U = \sum_{j=0}^{23} P_j \quad (2.9)$$

The PRFs directly scale the contribution of previous fluxes (in the form of temperature gradients) to the current conduction heat flux. As a result, the PRF series provides a visual representation of the thermal response of the wall. As shown in Figures 2.2, wall 17 has a slower thermal response than roof 10 because it is a more thermally massive construction.

PRFs are directly related to CTFs as shown in equation (2.10) (Spitler, et al. 1999) and may be derived directly from CTFs. The Toolkit uses this method to calculate PRFs.

$$P = d^{-1}b \quad (2.10)$$

As shown in equation (2.10), the PRFs are related to the cross and flux CTF terms. The first column of the  $P$  matrix is the resulting PRFs,  $P_0, P_1, P_2, \dots, P_{23}$ . Since the sol-air temperature is used in RTSM conduction calculations, the  $b$  and  $d$  matrices must be filled with air-to-air CTFs. This eliminates the surface heat balance calculations in the RTSM. However, if conduction heat transfer is an isolated concern, the PRFs can be calculated from surface-to-surface CTFs. This reflects the actual conduction response of a construction without considering the outside and inside film coefficients.

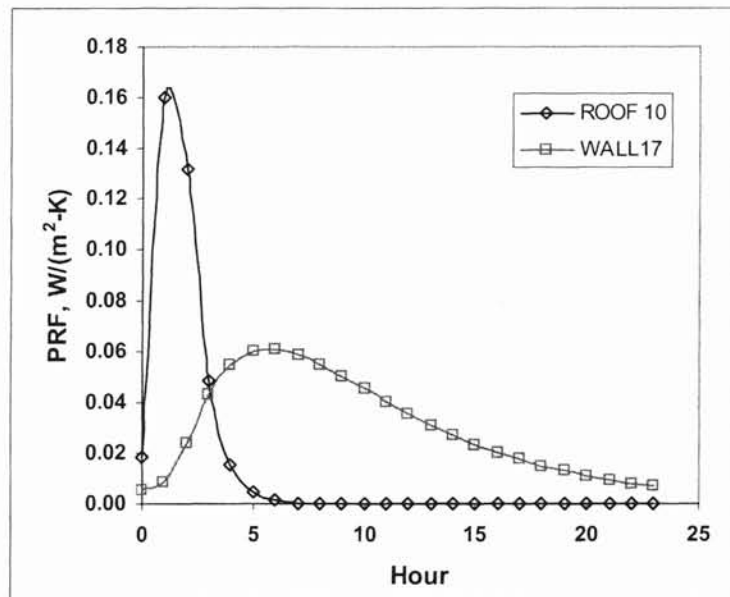


Figure 2.2 Periodic response factors for Roof 10 and Wall 17.

Using the Roof 10 Laplace CTFs listed in table 1, the resulting  $d$  and  $b$  matrices are shown below.

$$\mathbf{d} = \begin{pmatrix} 1 & 0 & \cdots & \cdots & \cdots & -2.95287743\text{E-}02 & 3.90083134\text{E-}01 \\ 3.90083134\text{E-}01 & 1 & 0 & \cdots & \cdots & 0 & -2.95287743\text{E-}02 \\ -2.95287743\text{E-}02 & 3.90083134\text{E-}01 & 1 & 0 & \cdots & \cdots & 0 \\ 0 & -2.95287743\text{E-}02 & 3.90083134\text{E-}01 & 1 & 0 & \cdots & 0 \\ 0 & 0 & -2.95287743\text{E-}02 & 3.90083134\text{E-}01 & 1 & \cdots & 0 \\ \vdots & \vdots & \vdots & \vdots & \vdots & \ddots & \vdots \\ 0 & 0 & \cdots & 0 & -2.95287743\text{E-}02 & 3.90083134\text{E-}01 & 1 \end{pmatrix}$$
  

$$\mathbf{b} = \begin{pmatrix} 1.79231787\text{E-}02 & 0 & \cdots & \cdots & 2.25362542\text{E-}03 & 7.00275192\text{E-}02 & 1.52697088\text{E-}01 \\ 1.52697088\text{E-}01 & 1.79231787\text{E-}02 & 0 & \cdots & \cdots & 2.25362542\text{E-}03 & 7.00275192\text{E-}02 \\ 7.00275192\text{E-}02 & 1.52697088\text{E-}01 & 1.79231787\text{E-}02 & 0 & \cdots & \cdots & 2.25362542\text{E-}03 \\ 2.25362542\text{E-}03 & 7.00275192\text{E-}02 & 1.52697088\text{E-}01 & 1.79231787\text{E-}02 & 0 & \cdots & 0 \\ 0 & 2.25362542\text{E-}03 & 7.00275192\text{E-}02 & 1.52697088\text{E-}01 & 1.79231787\text{E-}02 & \cdots & 0 \\ \vdots & \vdots & \vdots & \vdots & \vdots & \ddots & \vdots \\ 0 & 0 & \cdots & 2.25362542\text{E-}03 & 7.00275192\text{E-}02 & 1.52697088\text{E-}01 & 1.79231787\text{E-}02 \end{pmatrix}$$

After taking the inverse of  $\mathbf{d}$ , and calculating  $\mathbf{d}^{-1}\mathbf{b}$ , the  $\mathbf{P}$  matrix is calculated. Table 2.3 lists the first column of the  $\mathbf{P}$  matrix, i.e. PRFs of Roof 10 from Laplace CTFs. Other PRFs derived from tables 1 and 2 are also listed in tables 2.3 and 2.4, respectively. The overall heat transfer coefficients of both constructions were calculated using equation (2.9) and are also shown for comparison. Since U-value must be unique for any construction, regardless of whether it is calculated using PRFs or CTFs, the predicted U-values should be identical. Note that the PRF U-values are almost identical to the CTF U-values that are shown in tables 2.1 and 2.2. The differences are due to round off in the PRF calculation. While the CTFs can be different for an identical slab, PRFs theoretically must be unique for any slab. Figure 2.3 illustrates that the PRFs for Roof 10 and Wall 17 are the same when calculated from state-space and Laplace CTFs. The numeric differences for the corresponding PRFs shown in tables 2.3 and 2.4 are to be expected since the methods used to determine the state-space and Laplace CTFs are different.

Table 2.3 Periodic response factors of Roof 10 (W/m<sup>2</sup>-K).

ASHRAE Toolkit (State-space)				ASHRAE Toolkit (Laplace)			
$P_0$	1.84341408E-02	$P_{12}$	7.38448080E-07	$P_0$	1.79231800E-02	$P_{12}$	7.35175100E-07
$P_1$	1.59932405E-01	$P_{13}$	2.12324096E-07	$P_1$	1.59688600E-01	$P_{13}$	2.11220500E-07
$P_2$	1.31251603E-01	$P_{14}$	6.10487234E-08	$P_2$	1.31790100E-01	$P_{14}$	6.06847500E-08
$P_3$	4.87761796E-02	$P_{15}$	1.75530701E-08	$P_3$	4.89473200E-02	$P_{15}$	1.74350100E-08
$P_4$	1.51683800E-02	$P_{16}$	5.04695397E-09	$P_4$	1.52019200E-02	$P_{16}$	5.00915800E-09
$P_5$	4.47941804E-03	$P_{17}$	1.45112800E-09	$P_5$	4.48465900E-03	$P_{17}$	1.43915400E-09
$P_6$	1.30014296E-03	$P_{18}$	4.17235996E-10	$P_6$	1.30049600E-03	$P_{18}$	4.13475300E-10
$P_7$	3.75083386E-04	$P_{19}$	1.19965898E-10	$P_7$	3.74875000E-04	$P_{19}$	1.18793300E-10
$P_8$	1.07975997E-04	$P_{20}$	3.44932485E-11	$P_8$	1.07830400E-04	$P_{20}$	3.41298400E-11
$P_9$	3.10592695E-05	$P_{21}$	9.91768299E-12	$P_9$	3.09932000E-05	$P_{21}$	9.80565500E-12
$P_{10}$	8.93171364E-06	$P_{22}$	2.85158507E-12	$P_{10}$	8.90582900E-06	$P_{22}$	2.81720800E-12
$P_{11}$	2.56823705E-06	$P_{23}$	8.19903119E-13	$P_{11}$	2.55882200E-06	$P_{23}$	8.09396400E-13
<b>U-values</b>	3.79868925E-01			3.79862470E-01			

Table 2.4 Periodic response factors of Wall 17 (W/m<sup>2</sup>-K).

ASHRAE Toolkit (State-space)				ASHRAE Toolkit (Laplace)			
$P_0$	5.76257706E-03	$P_{12}$	3.53873298E-02	$P_0$	5.76430100E-03	$P_{12}$	3.53839000E-02
$P_1$	8.34633410E-03	$P_{13}$	3.09756696E-02	$P_1$	8.20602900E-03	$P_{13}$	3.09755400E-02
$P_2$	2.41068397E-02	$P_{14}$	2.69579198E-02	$P_2$	2.40656400E-02	$P_{14}$	2.69606300E-02
$P_3$	4.29386906E-02	$P_{15}$	2.33521406E-02	$P_3$	4.30147300E-02	$P_{15}$	2.33571400E-02
$P_4$	5.48282117E-02	$P_{16}$	2.01518796E-02	$P_4$	5.48862700E-02	$P_{16}$	2.01586300E-02
$P_5$	6.00564107E-02	$P_{17}$	1.73359308E-02	$P_5$	6.00801600E-02	$P_{17}$	1.73439400E-02
$P_6$	6.07338399E-02	$P_{18}$	1.48749799E-02	$P_6$	6.07353900E-02	$P_{18}$	1.48838200E-02
$P_7$	5.85691705E-02	$P_{19}$	1.27359899E-02	$P_7$	5.85597300E-02	$P_{19}$	1.27452900E-02
$P_8$	5.47539406E-02	$P_{20}$	1.08850496E-02	$P_8$	5.47407000E-02	$P_{20}$	1.08945000E-02
$P_9$	5.00902496E-02	$P_{21}$	9.28912964E-03	$P_9$	5.00773600E-02	$P_{21}$	9.29851600E-03
$P_{10}$	4.51054499E-02	$P_{22}$	7.91719276E-03	$P_{10}$	4.50950600E-02	$P_{22}$	7.92633400E-03
$P_{11}$	4.01360206E-02	$P_{23}$	6.74070278E-03	$P_{11}$	4.01290400E-02	$P_{23}$	6.74947000E-03
<b>U-values</b>	7.22031650E-01			7.22032120E-01			



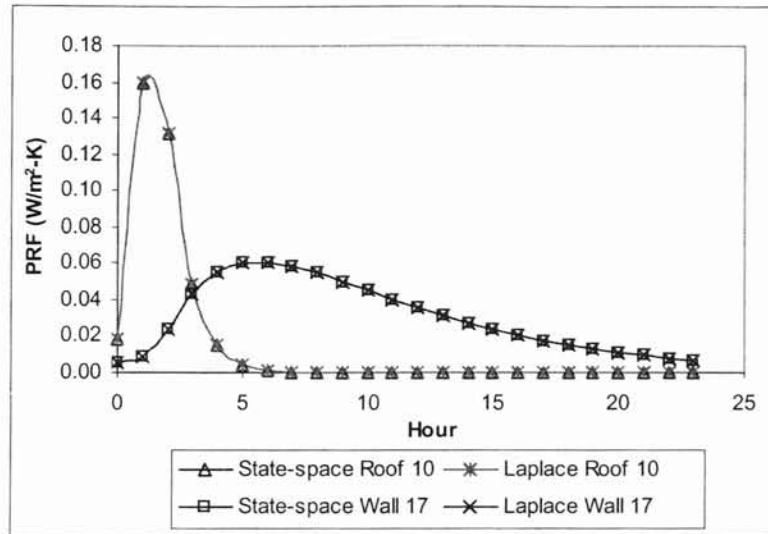


Figure 2.3 Comparisons of State-space and Laplace PRFs.

## 2.3 Using the Toolkit Modules to Calculate CTFs and PRFs

To facilitate the evaluation and validation of the CTF and PRF calculations, and to illustrate the utility of the ASHRAE Loads Toolkit, the Toolkit CTF modules were used to generate CTFs and PRFs. Each ASHRAE Loads Toolkit module contains a set of subroutines and functions required to achieve its computational objective. The following sections describe the incorporation of the CTF modules in a stand-alone program that generates CTFs and PRFs.

### 2.3.1 Overview of the algorithm

The algorithm consists of a driver program that first calls the Toolkit CTF routines to calculate CTFs then converts the CTFs to PRFs by applying equation (2.10). The required surface construction information is in standard Toolkit input file format and

is read using the Toolkit input processor as described by Crawley et al. (1998). The overall procedure is shown in figure 2.4 and can be summarized as follows:

- Get the surface and construction information from the input file.
- Pass this information to the CTF computational module and calculate CTFs.
- Print the CTF results to an output file.
- Convert the CTFs to PRFs.
- Print the resulting PRFs to another output file.

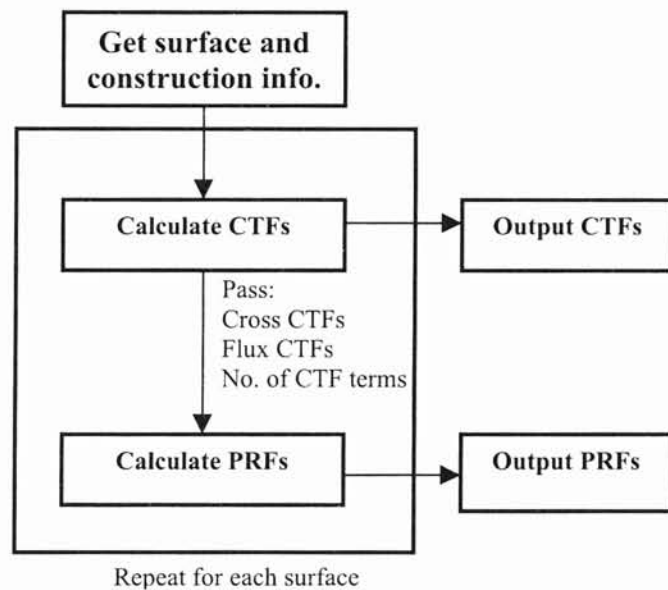


**Figure 2.4 CTF and PRF calculation framework.**

### 2.3.2 Structure of the Algorithm

The structure of the algorithm for CTF and PRF calculations is shown in figure 2.5. The “USE” statement is a Fortran 90 key word that makes the subroutines in a FORTRAN 90 module available to a program, subroutine or another module. “USE” is followed by the Toolkit module name. Subroutines in one FORTRAN 90 module cannot be “called” by another module unless the calling routine or module “uses” the target

module. The module “InputProcessor” handles all input data. The data is organized under keywords with a one-to-one correspondence between each definition and data value. The keywords for calculating CTFs and PRFs are SURFACE, CONSTRUCTION and MATERIALLAYER. Table 2.5 shows the required data for each keyword. By changing the data values of these keywords, the Toolkit generates different CTFs and PRFs. Although manual construction of a Toolkit input data file is tedious, the structured input format is conducive to the application of a graphical user interface as discussed in section 2.4.

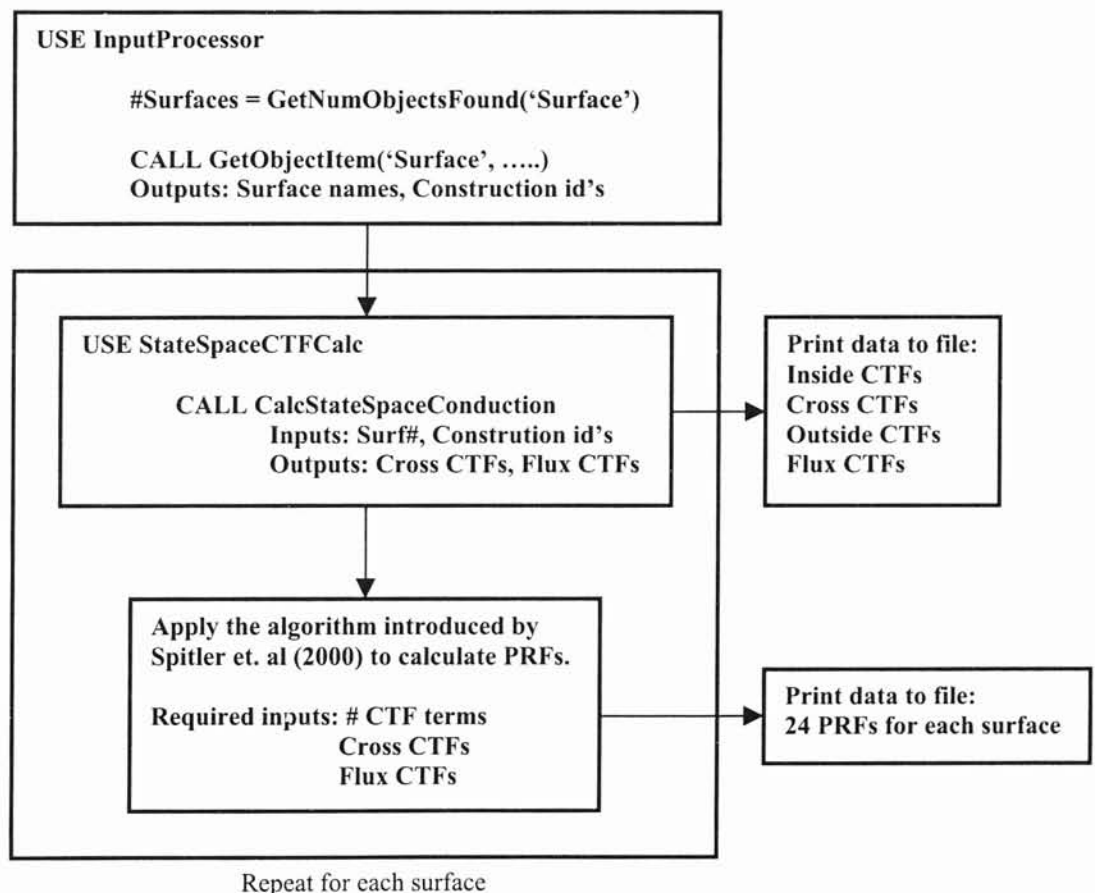


Figure 2.5 Structure of the toolkit CTF and PRF calculations.

**Table 2.5 Required data values in the toolkit input file for CTF and PRF calculation.**

<b>Keyword</b>	<b>Required Data</b>
SURFACE	Surface name; construction id
CONSTRUCTION	Construction name; layer names
MATERIALLAYER	Layer names; thickness, thermal conductivity, density, specific heat or thermal resistance

The function “GetNumObjectsFound” and the subroutine “GetObjectItem” in this module are used in the CTF and PRF calculations. “GetNumObjectsFound” returns the number of surfaces in the calculations, while “GetObjectItem” returns two arrays containing all data values (numeric and alpha) for the keyword “Surface”. Although there will be a number of surface data values returned from this subroutine, only the surface name and the construction ID are useful for the calculations. The argument variables of this subroutine are described in the Toolkit documentation (ASHRAE, 2001). In a similar way, the data associated with the keywords CONSTRUCTION and MATERIALLAYER are read into the program.

The program can be configured to use either the state-space or the Laplace CTF module. Figure 2.5 shows the program configured to use the “StateSpaceCTFCalc” module. It contains subroutines that import the construction and material layer data, generates CTFs and performs related calculations. The subroutine “CalcStateSpaceConduction” is the main calling routine of this module. It was modified to obtain the desired output format of the CTFs and to facilitate calculation of PRFs. The inputs to this subroutine are surface number and construction names. The surface number is assigned in order of appearance of the surface data in the input file; construction names are identifiers for each set of data and are used to map the construction data to a specific surface in the computational algorithm.

The inputs to the PRF subroutine are the number of CTF terms and the cross and flux CTFs. This data is used to fill the  $\mathbf{b}$  and  $\mathbf{d}$  matrices shown in equation (2.10). FORTRAN matrix functions are used to calculate the PRFs and the results are printed to an output file. If the PRFs are to be used in the RTSM, air resistance layers must be included at both inside and outside of the construction specification in the input file. Once the air resistance layers have been added, the resulting CTFs and PRFs will be air-to-air type, as described in section 2.2. Typical inside and outside resistance values for vertical surfaces are 0.12 and 0.04 (m<sup>2</sup>-K)/W or 0.68 and 0.25 (hr-ft<sup>2</sup>-F)/Btu, respectively (ASHRAE, 2001). The air-to-air PRFs can be directly applied to the RTSM, however the air-to-air CTFs cannot be used in the HBM since the inside and outside convection coefficients are already included in the heat balance calculations.

## **2.4 The Toolkit User Interface to CTF and PRF generator**

To facilitate calculation of CTFs and PRFs, a simple user interface to the FORTRAN 90 program was developed. This interface and a compiled version of the program can be downloaded from [www.hvac.okstate.edu](http://www.hvac.okstate.edu) and freely used for any purpose. The Toolkit program was compiled into a dynamic link library (DLL) file. When this file is called from the interface, it imports data from the input file, generates CTFs and PRFs and prints them to separate output files. The inputs to this DLL file are the names of the Toolkit idd and idf files. The interface allows the user to display the output on a spreadsheet or notepad for further application or analysis. In addition, related information including surface names, constructions and U-values are displayed by the interface.

The dialog box shown in figure 2.6 guides the user in creating a valid Toolkit input file by requesting the definition of surface names, number of layers and material properties. The number of material layers is limited by the Toolkit algorithm to ten. Material layer data are entered from outside to inside. Material layers can be either resistive as illustrated by layer F01 or completely specified as illustrated by layer G03 in figure 2.6. It should be noted that only fully specified layers capture the expected “lag and decrement” effect of thermal mass. The resistance layer option should only be used for material layers with low thermal capacitance. This primarily applies to air layers, but is often also applied to glazing.

Layer Name	Thickness mm	Conductivity W/(m·K)	Density kg/m <sup>3</sup>	Specific Heat kJ/(kg·K)	Resistance [m <sup>2</sup> ·K)/W	
1 F01					0.040	Edit
2 F13	9.500	0.160	1120.000	1.460		Edit
3 G03	12.700	0.070	400.000	1.300		Edit
4 I02	50.800	0.030	43.000	1.210		Edit
5 F08	0.762	45.284	7832.773	0.502		Edit
6 F05					0.180	Edit
7 F16	13.100	0.060	368.000	0.590		Edit
8 F03					0.160	Edit

Note: Enter the outside layer first.  
Enter either thickness, conductivity, density, specific heat or resistance.  
For air-to-air PRF, outside and inside surface resistances should be input as the first and last layers respectively.

Figure 2.6 Dialog box used for creating toolkit input file.

The default layer type of fully specified properties, can be changed by clicking the “Edit” button. For input convenience, an ASHRAE material database which contains the data shown in table 22, chapter 29, ASHRAE Handbook of Fundamentals 2001 (ASHRAE, 2001) is included as shown in figure 2.7. This database can be modified and

saved for future reference. The interface can handle up to 100 surfaces, which may be specified in either SI or IP units. All IP unit data is converted to SI units by the interface before writing the input file, since input to the Toolkit modules must be in consistent SI units and in accordance with Toolkit conventions.

The screenshot shows a window titled "Material Database" with a menu bar containing "Select", "Edit", "Add", "Delete", "Save", and "Close". Below the menu bar, there are labels for various material properties: Thickness - mm, Density - kg/m<sup>3</sup>, Resistance - (m<sup>2</sup>K)/W, Thermal Capacity - kJ/(m<sup>2</sup>K), Conductivity - W/(m-K), Specific Heat - kJ/(kg-K), Mass - kg/m<sup>2</sup>, and a "Notes" column. The main area of the window contains a table with the following data:

ID	Description	Thickness	Conductivity	Density	Specific Heat	Resistance	Mass	Thermal Capacity	Notes
F01	Outside Surface Resistance	0	0	0	0	0.044			1
F02	Inside Vertical Surface Resistance	0	0	0	0	0.12			2
F03	Inside Horizontal Surface Resistance	0	0	0	0	0.162			3
F04	Wall Air Space Resistance	0	0	0	0	0.153			4
F05	Ceiling Air Space Resistance	0	0	0	0	0.176			5
F06	EIFS Finish	9.525	0.721	1858.081	0.837	0.013	17.698	14.813	6
F07	Tin Stucco	25.4	0.721	1858.081	0.837	0.035	47.195	39.502	6
F08	Metal Surface	0.762	45.284	7832.773	0.502	0	5.969	2.996	7
F09	Opaque Spandrel Glass	6.35	0.995	2530.835	0.879	0.006	16.071	14.126	8
F10	1 in Stone	25.4	3.173	2562.87	0.795	0.008	65.097	51.752	9
F11	Wood Siding	12.7	0.089	592.664	1.172	0.143	7.527	8.822	10
F12	Asphalt Shingles	3.175	0.041	1121.256	1.256	0.077	3.56	4.471	
F13	Built-up Roofing	9.525	0.162	1121.256	1.465	0.059	10.68	15.646	
F14	Slate or Tile	12.7	1.586	1922.153	1.256	0.008	24.411	30.66	
F15	Wood Shingles	6.35	0.038	592.664	1.298	0.167	3.763	4.884	
F16	Acoustic Tile	19.05	0.061	368.413	0.586	0.312	7.018	4.113	11
F17	Carpet	12.7	0.058	288.323	1.381	0.219	3.662	5.057	12
F18	Terrazzo	25.4	1.803	2562.87	0.795	0.014	65.097	51.752	13
G01	5/8 in Gyp Board	15.875	0.16	800.897	1.088	0.099	12.714	13.833	
G02	5/8 in Plywood	15.875	0.115	544.61	1.214	0.138	8.646	10.496	
G03	1/2 in Fiberboard Sheathing	12.7	0.068	400.449	1.298	0.187	5.086	6.602	14
G04	1/2 in Wood	12.7	0.153	615.089	1.632	0.083	7.812	12.749	15

Figure 2.7 Material database.

## 2.5 Evaluation of the Program Outputs

The PRF generator can efficiently and conveniently calculate the desired CTFs and PRFs for any construction. This section establishes the validity of the program in terms of the self-consistency of the program outputs, the agreement of program output with previously published data and the conservation of energy based on a steady state test.

### 2.5.1 Consistency of PRFs and CTFs

Since the U-value is unique for any construction, and since it can be calculated either using CTFs or PRFs, the U-value check can be used to evaluate the program algorithm that converts CTFs to PRFs. Figure 2.8 compares the U-values calculated by CTFs and PRFs for the wall and roof database used by Spitler et al. (2000). The diagonal line represents a zero percent difference between the two. The results show nearly perfect agreement between the CTF and PRF U-values. The differences show up in the 5<sup>th</sup> decimal place, and are probably due to round-off error.

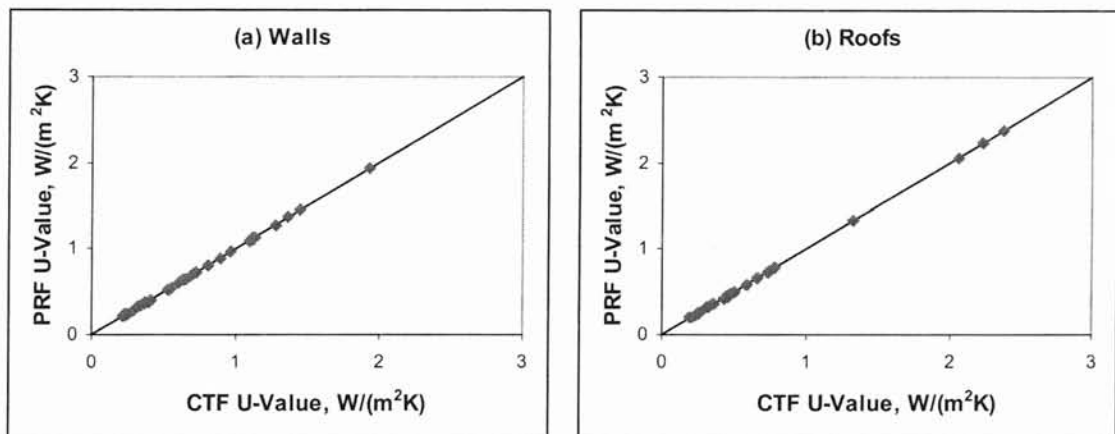


Figure 2.8 Comparisons of U-values.

### 2.5.2 Comparison with Published Data

The second step in evaluating program output is based on the fact that the PRF series is unique for any construction regardless of whether it is derived from state-space or Laplace CTFs. Since a PRF database for the HOF walls and roofs is already available in the literature (Spitler et al. 2000), the validity of the program outputs is evaluated by a term by term comparison of calculated and published PRFs for each construction, as



shown in figure 2.9. The small differences shown in the figure could be caused by slight numerical differences in the input data, the type of CTFs used to derive PRFs, as well as the round-off error in both calculations. In addition, if the convergence criterion used in the CTF calculation is different from that used by Spitler et al. (2000), it would also cause the numerical difference in the PRFs. In general, the program outputs agree very well with the published data.

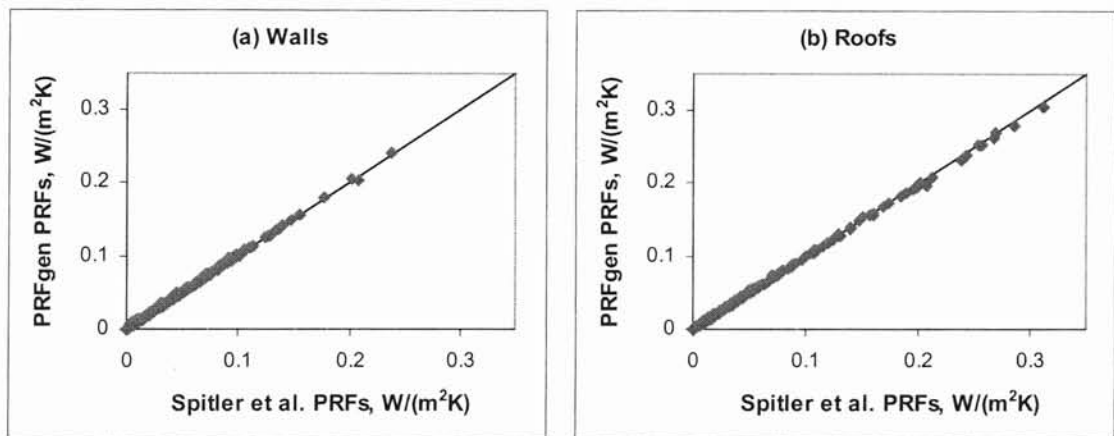


Figure 2.9 Comparison of the PRF generator outputs to the PRF database of Spitler et al. (2000)

### 2.5.3 Steady State Evaluation

The program outputs for a given construction can also be verified at the steady-state limit by comparing the U-value predicted by the CTFs or PRFs with that predicted by the steady state calculation. At steady state, the U-value is calculated as follows.

$$U = \frac{1}{R_T} \quad (2.11)$$

The thermal resistance for each layer is calculated as,

$$R = \frac{1}{h} \text{ for air resistance layer} \quad (2.12)$$

$$R = \frac{L}{k} \text{ for thermal mass layer} \quad (2.13)$$

Therefore, the total thermal resistance is

$$R_T = \sum_{i=1}^n R_i \quad (2.14)$$

If the calculated U-value from the steady-state equation (2.14) is equal to that from the CTFs and PRFs, energy is conserved. Figure 2.10 shows the comparison of the program output U-values with the steady-state U-values based on the same construction database used by Spitler et al. (2000). The U-values shown on the vertical axis are the PRF U-values from figure 2.8.

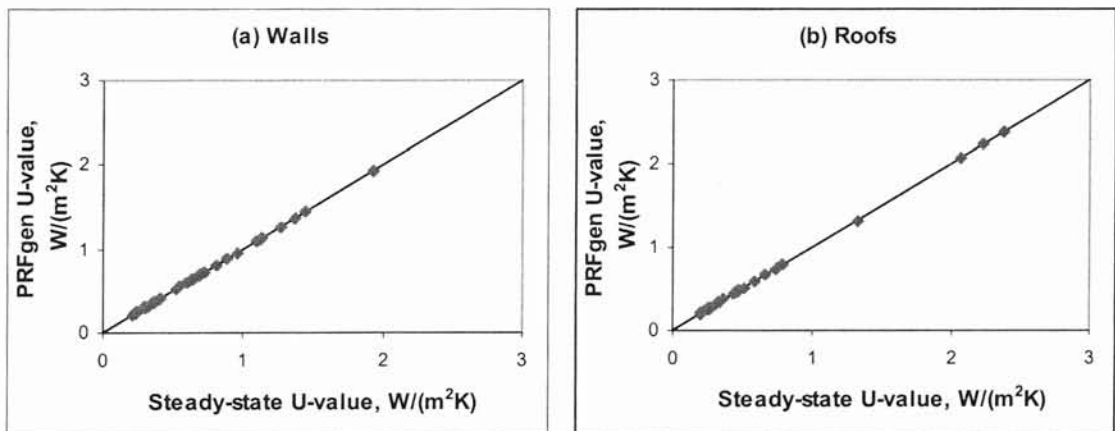


Figure 2.10 Comparison of the PRF generator U-values to the steady-state U-values.

Figure 2.10 shows that the use of the program outputs to calculate U-values are satisfactory. The steady-state U-values agree with the calculated U-values to within  $\pm 3.4\%$ . Although some round-off error is expected, the root cause of the differences is primarily due to the convergence criteria used in the Toolkit module. The CTFs calculated from the computer program are based on the default Toolkit settings. A better result is obtained if one tightens the convergence criteria in the Toolkit CTF module.

The steady-state evaluation is necessary but not sufficient to guarantee the accuracy of the transient calculation. A more rigorous transient evaluation that applies a sinusoidal temperature variation to the outside surface and a constant temperature to the inside surface and compares the resulting heat flux to the analytical solution presented in ASHRAE RP-1052 (Spitler et. al 2001) is presented in the next chapter. However, for most standard constructions, the steady state test is a good indicator of CTF and PRF accuracy.

## **2.6 Uncertainty Analysis of Conduction to Cooling Load Calculation**

To quantify the error propagated to the cooling load due to error in the CTF/PRF calculation, an uncertainty analysis was performed based on a worst case scenario residential type buildings. Four geometrically identical buildings are used for the analysis. They are described below:

LW 10% - Light weight, with 10% glazed area on south and west surfaces

LW 50% - Light weight, with 50% glazed area on south and west surfaces

HW 10% - Heavy weight, with 10% glazed area on south and west surfaces

HW 50% - Heavy weight, with 50% glazed area on south and west surfaces

All surfaces except the floor are exposed to the environmental conditions. No internal load, infiltration rate is small (0.25 ACH) such that the cooling load is dominated by the building envelope influence. To study the error in total cooling load due to uncertainty in the CTFs, influence coefficients (ICs) were calculated based on a 5% perturbation of the

hourly PRFs of all surfaces. Figure 2.11 shows the perturbed PRFs compared to the based PRFs for one surface.

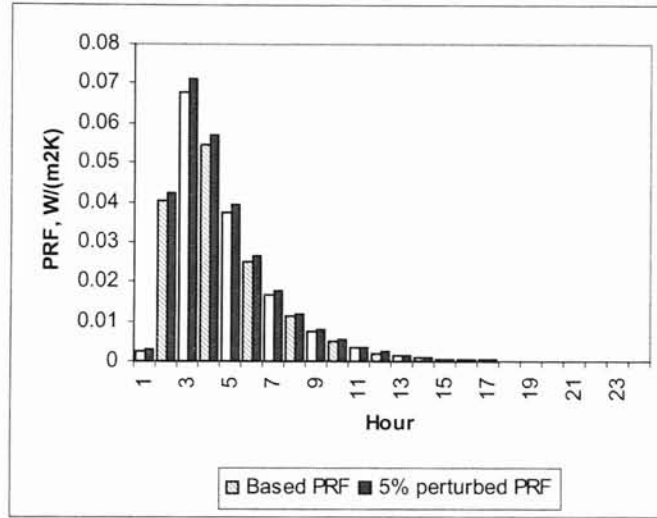


Figure 2.11 Perturbation of PRFs.

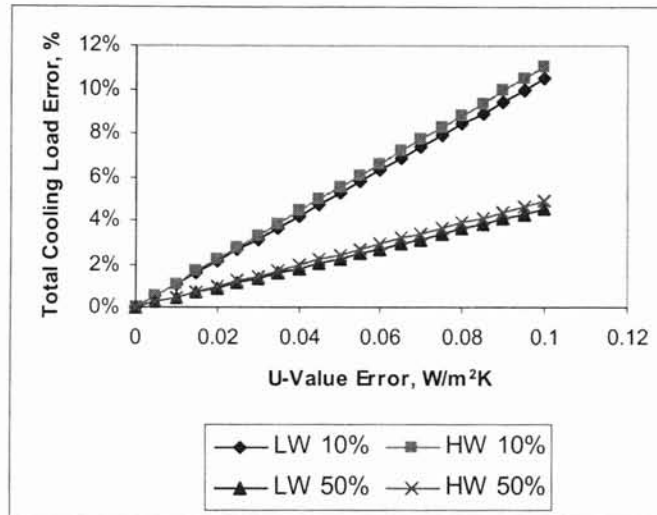
Since the sum of PRFs is always equal to the U-value, the perturbation of the PRFs is equivalent to the perturbation of the overall U-value of the building envelope under steady state condition. The resulting influence coefficients are listed in table 2.6.

Table 2.6 Influence coefficients of overall U-value to total cooling loads.

Building	LW 10%	HW 10%	LW 50%	HW 50%
ICs,%/(W/m <sup>2</sup> K)	1.05	1.10	0.45	0.49

The ICs can quantify the intuitive result of the influence of the CTF uncertainty to the cooling load. The higher values of ICs show that the conduction calculation is more influential on the cooling load for the buildings with 10% glazed area. For the buildings with 50% glazed area, the solar load dominates and the influence of conduction heat gain become less significant. Apart from the changes of glazed area, the ICs also show that the influence of conduction on the cooling load has a similar effect for light weight and

heavy weight buildings. Using the calculated ICs, figure 2.12 shows the approximate error in the the total cooling load due to the U-value error.



**Figure 2.12** The influence of the U-value error to the total cooling load error.

For a 0.02 W/(m<sup>2</sup>K) or 0.004 Btu/(hr-ft<sup>2</sup>-F) error of the U-value, the total cooling load error is 2% for buildings with less glazing, and is 1% for the highly glazed building envelopes. The cooling load error increases linearly with the U-value error. In the steady-state U-value verification discussed in the above section, the maximum U-value error is 0.01 W/(m<sup>2</sup>K) or 0.002 Btu/(hr-ft<sup>2</sup>-F), which is Wall 35, a concrete brick wall with insulation (ASHRAE, 1997). The exact U-value of this wall is 0.297 W/(m<sup>2</sup>K) or 0.052 Btu/(hr-ft<sup>2</sup>-F), and the PRF U-value is 0.287 W/(m<sup>2</sup>K) or 0.051 Btu/(hr-ft<sup>2</sup>-F), which is equivalent to a 3.5% error in U-value. Figure 2.12 shows that the error will result in a 1% error in the total cooling load for the 10% glazing buildings, and a 0.4% error for the 50% glazing buildings. Therefore, the relative error in U-value is not suitable to approximate the cooling load error. Depending on the relative amount of conduction heat gain

contributed in the building cooling load, the total cooling load error predicted by the U-value error changes accordingly.

## **2.7 Summary and Conclusions**

Transfer function and response factor methods continue to provide a robust, accurate and tractable approach to calculating conduction heat gains in cooling load procedures. Although care must be taken to consistently apply CTFs and PRFs depending on whether they were generated with or without a convective resistance layer, the application of boundary conditions and solution techniques is straightforward and consistent.

In the past, the most serious drawback to the use of transfer function and response factor methods was the complexity of the computer code required to generate the coefficients. The ASHRAE Loads Toolkit addresses this problem by providing the source code required to generate conduction transfer functions and periodic response factors for arbitrary wall or roof constructions. The computational algorithm required to implement the toolkit modules in a CTF/PRF generator program was presented in the chapter. In addition, input/output and interface issues were discussed. The CTFs and PRFs calculated by the Toolkit algorithms can be directly applied to heat balance and radiant time series load calculation procedures.

The outputs of the computer program were evaluated based on the physical significance of the CTFs and PRFs and were compared to the published literature. A simple method for checking the steady state accuracy of CTFs and PRFs was also used in the evaluation. The results showed that the outputs are satisfactory. An uncertainty

analysis was performed to show the influence of the U-value error on the resulting cooling load. For the test cases, a 0.01 W/(m<sup>2</sup>K) or 0.002 Btu/(hr-ft<sup>2</sup>-F) (3.4%) error in U-value resulted in less than a 1.5% error in the cooling load.

## CHAPTER 3

# BOUNDING THE RANGE OF APPLICABILITY OF CONDUCTION TRANSFER FUNCTION METHODS IN COOLING LOAD AND ENERGY CALCULATIONS

### 3.1 Introduction

Since CTFs are temperature independent, they are usually calculated during program initialization and may be saved in a library or database. Pre-calculated CTFs for typical constructions are available in the literature (ASHRAE, 1997). Due to the convenience and ease with which it may be implemented, the CTF method is often used indiscriminately in cooling load and energy calculations without due consideration of either the required convergence criterion of the solution technique or the inherent inaccuracies of the CTFs for a particular application. As addressed in the previous chapter, periodic response factors (PRFs) are closely related to CTFs. This chapter identifies the sources of error in calculating CTFs by the Laplace and state-space methods and compares CTF accuracy for a large parametric set of wall constructions.

### 3.2 Overview of the Solution Methods

While there are a number of numerical methods for solving the transient conduction equations, the Laplace transform method and the state space method are the most widely used in cooling load and energy calculations.



### 3.2.1 Laplace Transform Method

Hittle (1979) introduced a procedure to solve the conduction heat transfer governing equations (2.1) and (2.2) by using Laplace transform method. The system in the Laplace domain is shown in equation (3.1).

$$\begin{bmatrix} q_{in}''(s) \\ q_{out}''(s) \end{bmatrix} = \begin{bmatrix} \frac{D(s)}{B(s)} & \frac{-1}{B(s)} \\ \frac{1}{B(s)} & \frac{-A(s)}{B(s)} \end{bmatrix} \begin{bmatrix} T_i(s) \\ T_o(s) \end{bmatrix} \quad (3.1)$$

Response factors are generated by applying a unit triangular temperature pulse to the inside and outside surface of the multi-layered slab as shown in figure 3.1.

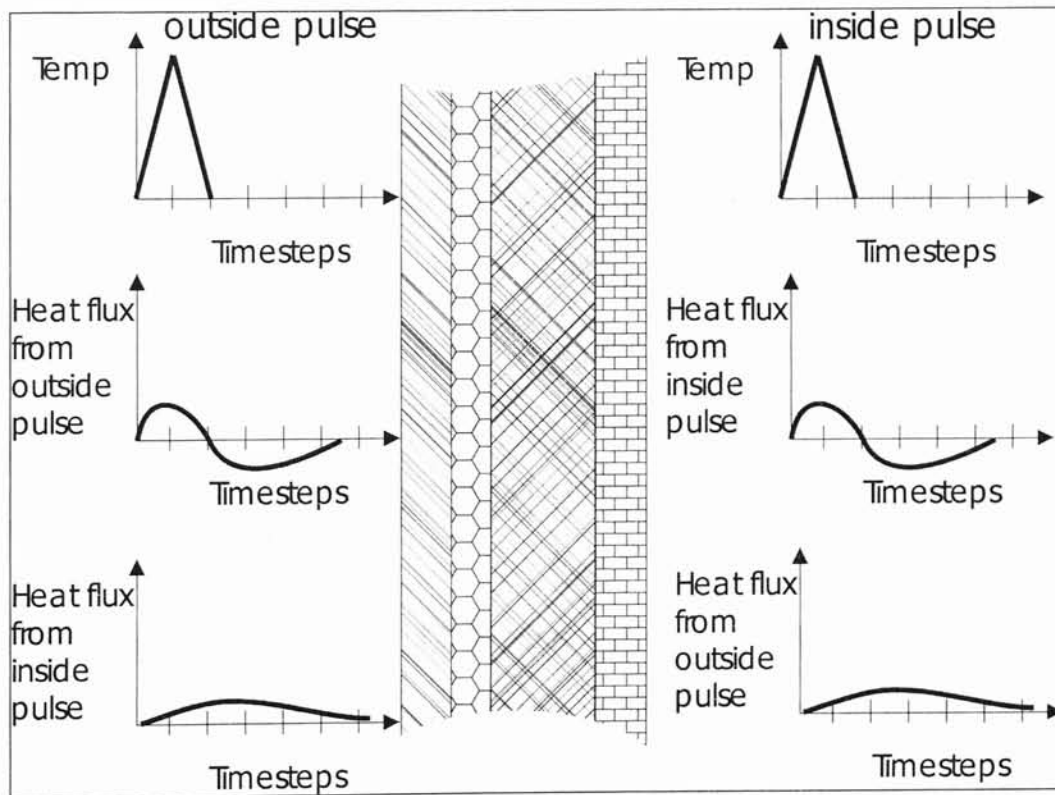


Figure 3.1 The generation of response factors.

The response factors are defined as an infinite series of discretized heat fluxes on each surface due to both an outside and inside temperature pulse. Hittle also described an algebraic operation to group response factors into CTFs, and to truncate the infinite series of response factors by the introduction of flux history coefficients. A convergence criterion shown below is used in the Laplace method to determine whether the numbers of CTFs and flux history coefficients are sufficient such that the resulting CTFs accurately represent the response factors.

$$\sum_{n=0}^{N_x} X_n = \sum_{n=0}^{N_y} Y_n = \sum_{n=0}^{N_z} Z_n = U \prod_{n=1}^{N_\phi} (1 - \phi_n) \quad (3.2)$$

where

$$N_x = N_y = N_z \quad (3.3)$$

The  $X_n$ ,  $Y_n$  and  $Z_n$  are exterior, cross and interior CTFs respectively. They are equivalent to CTFs shown in equations (2.3) and (2.4). The number of CTF terms will increase to satisfy the criteria shown in equation (3.2). Heavy weight (long thermal response time) constructions require more CTFs than light weight constructions.

The number of CTF terms can be determined in different ways. Mitalas (1978) suggests that the number of CTF terms should be:

$$N_x = N_y = N_z = I + N_\phi \quad (3.4)$$

and there is no limited number of CTF terms in this approach. Peavy (1978) suggests that the number of flux CTF terms should always be less than or equal to 5, even for thermally massive walls.

### 3.2.2 State-space Method

The use of the state-space method in solving the governing equations (2.1) and (2.2) was introduced by Seem (1987). The state-space expression is formulated by using either finite-difference or finite-element methods to discretize the governing equations. The state-space expression relates the interior and exterior boundary temperatures to the inside and outside surface heat fluxes at each node of a multi-layered slab as shown in equations (3.5) and (3.6).

$$\begin{bmatrix} dT_{is}/dt \\ \vdots \\ dT_{os}/dt \end{bmatrix} = a \begin{bmatrix} T_{is} \\ \vdots \\ T_{os} \end{bmatrix} + b \begin{bmatrix} T_i \\ T_o \end{bmatrix} \quad (3.5)$$

$$\begin{bmatrix} q_{ki}'' \\ \vdots \\ q_{ko}'' \end{bmatrix} = c \begin{bmatrix} T_{is} \\ \vdots \\ T_{os} \end{bmatrix} + d \begin{bmatrix} T_i \\ T_o \end{bmatrix} \quad (3.6)$$

The exterior and interior temperature variations,  $T_i$  and  $T_o$ , are modeled with piecewise linear functions. Equations (3.5) and (3.6) can be simplified using some matrix algebraic calculations, so that the surface heat fluxes are directly related to the surface and boundary temperatures only. This system of equations is solved directly for CTFs, without calculating response factors. The number of CTF terms is increased until the ratio of the last to the first flux history coefficient is less than a tolerance limit.

Since Laplace and state-space CTFs are calculated differently, the resulting CTFs are expected to be different even for the same slab. The number of CTF terms, and/or the numerical value of each single CTF can be different.

### 3.2.3 Analytical Method

The governing conduction equations (2.1) and (2.2) are usually not solved analytically in building thermal load and energy calculations due primarily to the computational intensity of the implementation. However, with a periodic temperature boundary condition on one side of the slab and a constant temperature boundary condition on the other side, the analytical solution is tractable. Spitler et al. (2001) presents an analytical solution for a multi-layered slab subject to a sinusoidal outside temperature and a constant inside temperature. For single-layered slabs of thickness  $L$ , the inside temperature and heat flux are related to the outside temperature and heat flux by the following set of equations:

$$\begin{bmatrix} T_i \\ q_{ki} \end{bmatrix} = \begin{bmatrix} m_1 & m_2 \\ m_3 & m_1 \end{bmatrix} \begin{bmatrix} T_o \\ q_{ko} \end{bmatrix} \quad (3.7)$$

where

$$m_1 = \cosh(p + jp) \quad (3.8)$$

$$m_2 = \frac{L \sinh(p + jp)}{k(p + jp)} \quad (3.9)$$

$$m_3 = \frac{k(p + jp) \sinh(p + jp)}{L} \quad (3.10)$$

$$\text{for a 24-hour cycle... } p = \left( \frac{\pi L^2 \rho c_p}{84600k} \right)^{0.5} \quad (3.11)$$

$$j^2 = -1 \quad (3.12)$$

For a resistive layer, equations (3.8) to (3.10) can be simplified as follows.

$$m_1 = L \quad (3.13)$$

$$m_2 = R \quad (3.14)$$

$$m_3 = 0 \quad (3.15)$$

The matrix formulation shown in equation (3.7) can be extended for multi-layered slabs with appropriate changes to the  $m$  matrix.

$$\begin{bmatrix} T_i \\ q_{ki}'' \end{bmatrix} = \begin{bmatrix} M_1 & M_2 \\ M_3 & M_1 \end{bmatrix} \begin{bmatrix} T_o \\ q_{ko}'' \end{bmatrix} \quad (3.16)$$

where:

$$\begin{bmatrix} M_1 & M_2 \\ M_3 & M_1 \end{bmatrix} = \begin{bmatrix} 1 & R_i \\ 0 & 1 \end{bmatrix} \begin{bmatrix} m_1 & m_2 \\ m_3 & m_1 \end{bmatrix}_{layer,1} \begin{bmatrix} m_1 & m_2 \\ m_3 & m_1 \end{bmatrix}_{layer,2} \dots \begin{bmatrix} m_1 & m_2 \\ m_3 & m_1 \end{bmatrix}_{layer,n} \begin{bmatrix} 1 & R_o \\ 0 & 1 \end{bmatrix} \quad (3.17)$$

$n$  = Number of layers

As a result, the so-called decrement factor and time lag can be calculated as follows:

$$f = \left| \frac{1}{UM_2} \right| \quad (3.18)$$

$$\phi = -\frac{1}{\omega} \tan^{-1} \left[ \frac{\text{Im}(f)}{\text{Re}(f)} \right] \quad (3.19)$$

where  $\omega = \frac{\pi}{12}$ , frequency of temperature boundary condition

The arctangent should be evaluated in the range of  $-\pi$  to 0 radians. For a sinusoidal outside temperature and a constant inside temperature, the inside heat flux can be formulated as:

$$q_{ki}''(t) = UfT_A \sin[\omega(t - \phi)] \quad (3.20)$$

The heat flux calculated from equation (3.20) is thus the exact solution of equations (2.1) and (2.2) for a sinusoidal temperature boundary condition.

### 3.3 Types and Sources of Errors in CTF Solution

Since CTFs are the products of numerical solution, numerical errors exist in the CTF solution. The errors come from the solution method used in solving the transient conduction equations and the applications of the CTFs in the conduction calculation. The following sections discuss the sources of errors in the CTF solution.

#### 3.3.1 Sources of Errors in CTF Calculation

This type of error sources is due to the numerical methods used in the CTF calculation. As the numerical methods: Laplace transform and state-space methods are concerned, the error sources are categorized into followings:

- **Root finding tolerance:** This error is only for the Laplace transform method. In order to calculate response factors, it is necessary to find the root of  $B(s) = 0$  in equation (3.1) (Hittle, 1979). Since the expression for  $B(s)$  becomes complicated for slabs with more than one layer, the root finding procedures rely on numerical method. The procedures iteratively continue until the root is found within a root finding tolerance or the maximum number of iterations is reached. The tolerance value and number of iterations can cause error in the CTF calculation.
- **Number of nodes:** This error is only for the state-space method that uses state-space nodes to discretize the transient conduction equations. Seem (1987) demonstrated that the CTF accuracy is dependent on the number of nodes specified. The CTF accuracy is proportional to the number of nodes used in each material layer in the calculation.
- **Number of CTF terms:** In the Laplace transform method, CTFs are derived from response factors and it is necessary to determine the number of CTF terms so that the

resulting CTFs can equivalently represent the response factors. Equation (3.2) is used to check the equivalence of response factors and CTFs. While in the state-space method, the number of CTF terms is determined by tracking the ratio of the last CTF flux term to the first term until the value is negligible. The number of CTF terms is determined with an iterative process until the conditions are satisfied within a tolerance limit or until the maximum number of iterations is reached. The tolerance value and number of iterations can introduce errors in the CTF calculation.

- **Solution time step:** CTFs are calculated based on an assumed temperature boundary condition. In the CTF calculation, the temperature variation is divided into time steps where the subset of temperature variation is approximated with linear temperature profiles. Therefore, this error is apparent when the time step is too large to approximate the temperature variation.

### 3.3.2 Sources of Errors in CTF Application

Besides the numerical values of the CTFs, the applications of the CTFs can also introduce error in the conduction calculation. The errors come from the following sources:

- **Solution Convergence:** Since conduction is a transient process, current heat flux is related to flux histories as shown in equations (2.3) and (2.4). The histories are generated using an iterative calculation. The conduction solution is assumed to be converged when the change of the history values in the iteration is less than a tolerance value. Therefore, the value of the tolerance limit and the number of iterations can cause error in the CTF conduction calculation.

- **Number of flux history terms:** Since the current heat flux is related to the flux histories, the number of flux history terms that are used in the calculation can alter the value of the current heat flux. The number of terms needed varies for different material properties. For light weight materials, the thermal response is fast and a few history terms are enough to accurately calculate the current heat flux, while for heavy weight materials, more terms are needed.

### 3.4 The Test Procedure

The test procedure presented in this section uses the analytical solution described in Section 3.2 to benchmark the accuracy of conduction calculations by the state-space and Laplace CTFs. Air-to-air CTFs (with constant inside and outside film coefficients) are calculated. The material properties and number of layers of the slab are varied over a wide range in order to investigate the range of applicability of the two methods. Figure 3.2 illustrates the boundary conditions and the calculated result of the test procedure. The steady, 24-hour periodic outside temperature,  $T_o$  is shown on the left hand side of the figure. The constant inside temperature,  $T_i$ , and the resulting inside surface heat flux are shown on the right hand side. The inside and outside film coefficients are treated as resistive layers. The sinusoidal outside air temperature profile is approximated for 1-hour time steps and 24-hour period as shown below. The inside air temperature is the mean air temperature,  $T_m$ .

$$T_o = T_m + T_A \sin\left(\frac{\pi}{12}t\right) \quad (3.21)$$



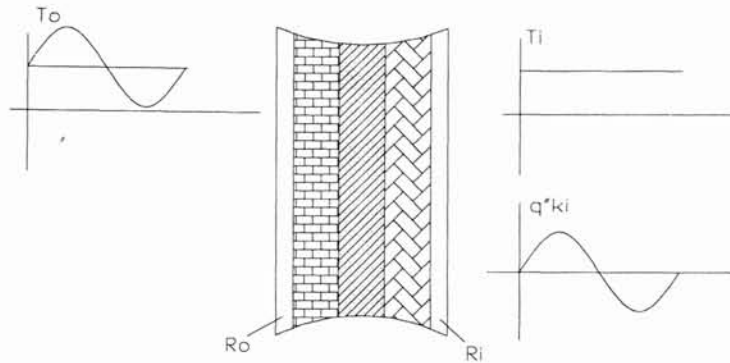


**Figure 3.2 CTF test procedure scheme.**

The ASHRAE Loads Toolkit (2001) algorithm was used to calculate the state-space and Laplace CTF solutions. The Toolkit minimizes the sources of error in the CTF solution with the default settings listed in table 3.1.

**Table 3.1 Default Toolkit settings for CTF solution.**

Error types	Error sources	Parameter settings	
		State-space CTF	Laplace CTF
CTF numerical error	(a) No. of state-space nodes	6 ~ 19	NA
	(b) Root finding tolerance	NA	1E-10
	(c) No. of CTF terms	TL = 1E-13 NI = Total no. of nodes < 18	TL = 1E-4 NI = No. of roots found ≤ 5
	(d) Solution time step	1 hour	1 hour
Application error	(e) Solution convergence*	TL = 1E-6 NI = 100	TL = 1E-6 NI = 100
	(f) No. of flux history terms	24	24

Note: NA = Not applicable  
 TL = Tolerance  
 NI = Number of iterations  
 \* = User defined parameters

Note that the solution convergence parameters of the application error are user-defined values. They are defined in the CTF driver subroutine written by Toolkit users. The tolerance value was chosen such that it is small enough to minimize the CTF application error. In this test, a large number of iterations were assigned to ensure converged solutions. The number of iterations of 4 for the CTF application is recommended for

general purposes (ASHRAE, 2001). The number of flux history terms is also a source of application error, but it is pre-set to 24 in the Toolkit algorithm. Therefore, users are required to change the Toolkit code in order to have more flux history terms in their conduction calculations. For the sources of CTF numerical error, users also need to modify the corresponding Toolkit code to alter the accuracy of the CTF solution.

In this test, the outside and inside surface film resistances shown in figure 3.2 are respectively equal to 0.059 and 1.205 (m<sup>2</sup>-K)/W or 0.334 and 0.685 (hr-ft<sup>2</sup>-F)/Btu. The mean air temperature is 20 C or 68 F, and the amplitude temperature is 15 C or 59 F. Using the default Toolkit CTF algorithm settings (Table 3.1), the test procedure starts with a single-layered slab with base material properties:

$$\begin{aligned} L &= 0.01 \text{ m or } 0.033 \text{ ft} \\ k &= 0.116 \text{ W/(m}^2\text{-K) or } 0.804 \text{ (Btu-in)/(hr-ft}^2\text{-F)} \\ \rho &= 540 \text{ kg/m}^3 \text{ or } 33.712 \text{ lbm/ft}^3 \\ c_p &= 1210 \text{ J/(kg-K) or } 0.289 \text{ Btu/(lbm-F)} \end{aligned}$$

The slab is subject to changes of layer thickness ( $L$ ), thermal conductivity ( $k$ ), density ( $\rho$ ) and specific heat ( $c_p$ ) until the CTF solutions fail to converge. The same test based on changing the material properties on each layer of multi-layered slabs is investigated afterward.

The error is calculated as the percent deviation of the numerical, CTF calculated heat flux from the analytical solution as follows:

$$E = \frac{q''_{num} - q''_{exact}}{q''_{exact}} \% \quad (3.22)$$

where  $q''_{exact}$  is the peak value of the 24-hour conduction heat fluxes calculated from analytical solution,  $q''_{num}$  is the conduction heat flux at the same time that  $q''_{exact}$  is calculated. Figure 3.3 shows how the error values are measured in the test. If CTF

numerical and application errors exist in the conduction calculation, any of the error characteristics shown in figure 3.3, or a combination of them could exist in the CTF solution.

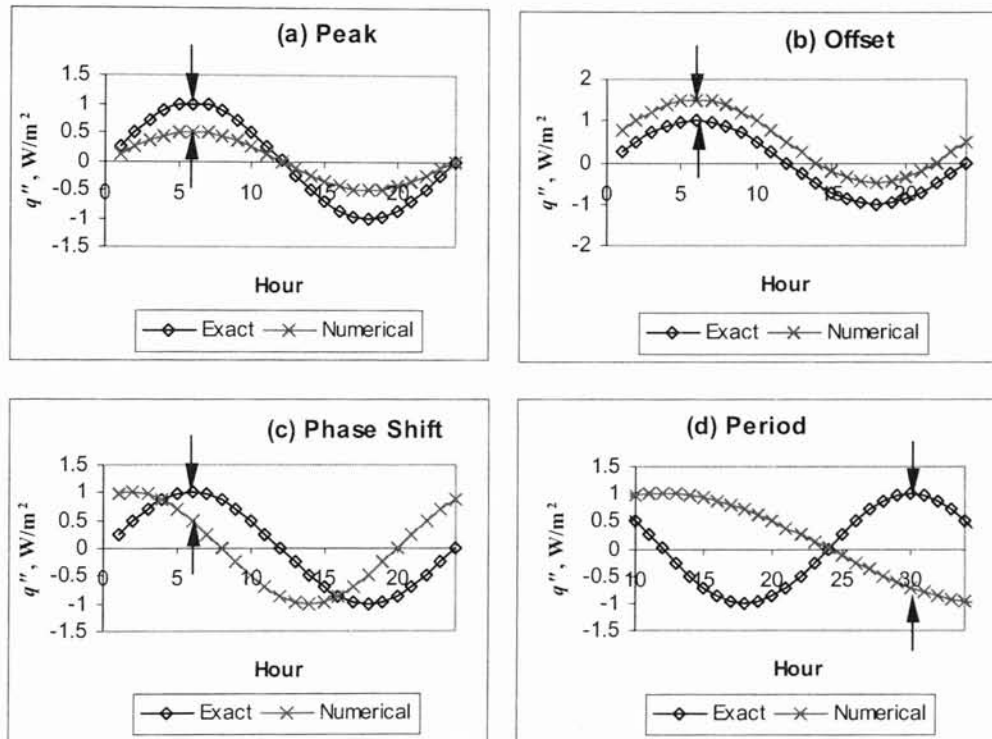


Figure 3.3 Error measured in the CTF solution test (Arrows indicate error).

### 3.5 Results and Discussions

This section presents the CTF solution test results on single- and multi-layered slabs. Since many convergence and tolerance checks are involved in the CTF calculations, in order to avoid confusion from the unconverged test results, the test results presented in this section only represent the CTF solutions that satisfy the convergence and tolerance values listed in table 3.1. For the CTF numerical error, warning messages are printed out from the Toolkit CTF algorithms to identify solutions that are not

converged. For the application error, Toolkit users are responsible for printing out warning messages from the driver subroutine to check the solution convergence.

### 3.5.1 Single-layered Slabs

Figure 3.4 shows the state-space and Laplace CTF solution errors as a function of the reciprocal of the Fourier number. Fourier number is defined as:

$$Fo = t/RC \quad (3.23)$$

where

$$R = L/k$$

$$C = L\rho c_p$$

Since the time step is constant in the CTF calculations, changes in the Fourier number represent changes in material properties only. Fourier numbers for heavy weight materials (larger  $R$  and  $C$ ) are smaller than Fourier numbers for lightweight materials. In other words, the value of  $1/Fo$  is larger for heavy weight materials. Figure 3.4 shows that the state-space CTF solutions always underpredict the peak heat flux, while the Laplace CTF solutions underpredict the heat flux for light weight materials but can also over estimate the heat flux for heavy weight materials. Since the errors show in figure 3.4 are calculated from converged solutions, the increase in the magnitude the error for the state-space CTF solution is due to the number of nodes defined in the calculations. The number of nodes in the Toolkit is calculated as:

$$N_{node} = \sqrt{\frac{1}{2Fo}} \quad (3.24)$$

where  $N_{node}$  is an integer and is limited to the following range in the Toolkit.

$$6 \leq N_{node} \leq 19$$

To reduce the CTF solution error for heavy weight materials, more than 19 nodes are required in the state-space CTF calculation. Compared to the error in state-space CTF solution, the error in the Laplace CTF solution becomes increasingly random as the material properties become more thermally massive. The randomness is due to a loose convergence criterion used in determining the number of CTF terms. Since the amount of conduction heat flux through heavy weight material is small, the error induced by the loose convergence criterion becomes significant.

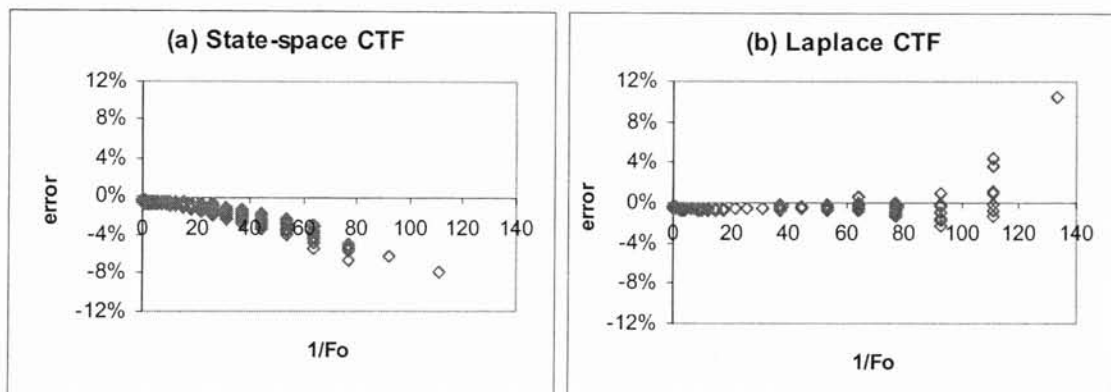


Figure 3.4 Single-layered CTF solution errors.

Figure 3.4 shows that the magnitude of the CTF solution errors is generally increasing from light weight to heavy weight materials. The maximum errors are  $-7.99\%$  for the state-space CTF solution, and  $10.38\%$  for the Laplace CTF solution. The hourly heat flux profiles for the largest error values are shown in figure 3.5. Note that although the errors are large, the peak flux differences are still small. The large error percentages are due to the small amount of conduction heat transfer through the heavy weight materials.

Figure 3.4 can be used to approximate the range of CTF solution errors in terms of the Fourier number. For any specific value of  $1/Fo$ , the CTF solution errors shown in

figure 3.4 can be further related to material properties. In case of  $1/Fo \approx 44.5$ , figure 3.6 shows the relationship between CTF solution errors and thermal resistance. Note that the errors can be more accurately approximated. An alternative way to view the errors is to use thermal capacitance. The resulting plots are similar to that showing in figure 3.6. Since the error ranges increase from light weight to heavy weight materials, constructing figure 3.6 to approximate CTF solution errors is especially useful for heavy weight material calculations.

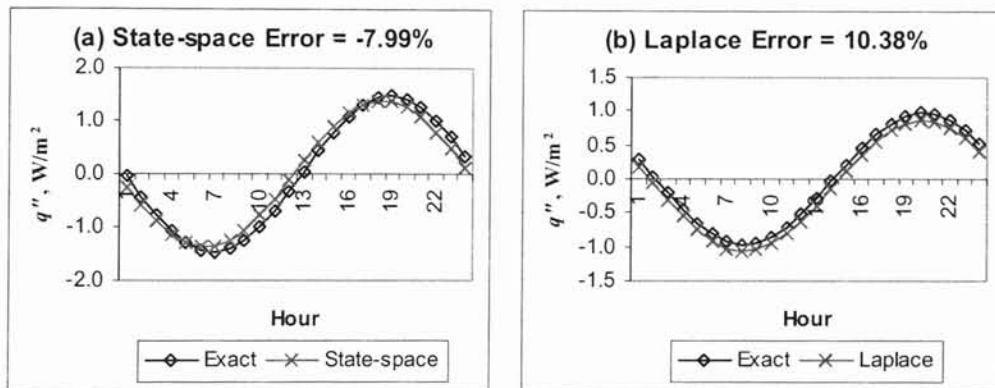


Figure 3.5 Maximum errors in the single-layered test.

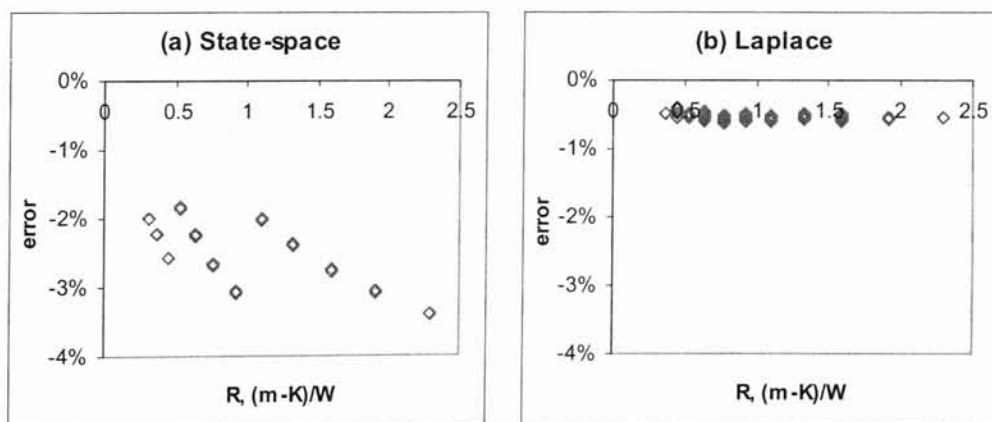


Figure 3.6 CTF solutions error for  $1/Fo \approx 44.5$ .

### 3.5.2 Multi-layered Slabs

The relationship of  $1/Fo$  to CTF solution errors shown above is only suitable for single-layered slabs. For multi-layered slabs, not only material properties, but also layer arrangement influences the CTF calculations. In order to take the layer arrangement into account, the thermal structure factor (Kossecka, 2000) is introduced. The thermal structure factor is related to the thermal resistance and capacity as shown below, where layer 1 is the interior layer.

$$S_{ie} = \frac{1}{R_T^2 C_T} \sum_{m=1}^n C_m \left( -\frac{R_m^2}{3} + \frac{R_m R_T}{2} + R_{i-m} R_{m-o} \right) \quad (3.25)$$

$$R_{i-m} = R_i + \sum_{k=1}^{m-1} R_k \quad (3.26)$$

$$R_{m-o} = R_o + \sum_{k=m+1}^n R_k \quad (3.27)$$

For single-layered slabs, the thermal structure factor can be simplified as:

$$S_{ie} = \frac{1}{6} + \frac{R_i R_o}{R^2} \quad (3.28)$$

Figure 3.7 shows the CTF solution errors as a function of  $1/(Fo \cdot S_{ie})$  for single-layered slabs. Note that due to the introduction of thermal structure factor, the error bands shown in figure 3.7 are smaller and more random in appearance than the error bands shown in figure 3.4. Figure 3.7 is therefore a better approximation of the range of CTF solution errors for the single-layered slab.

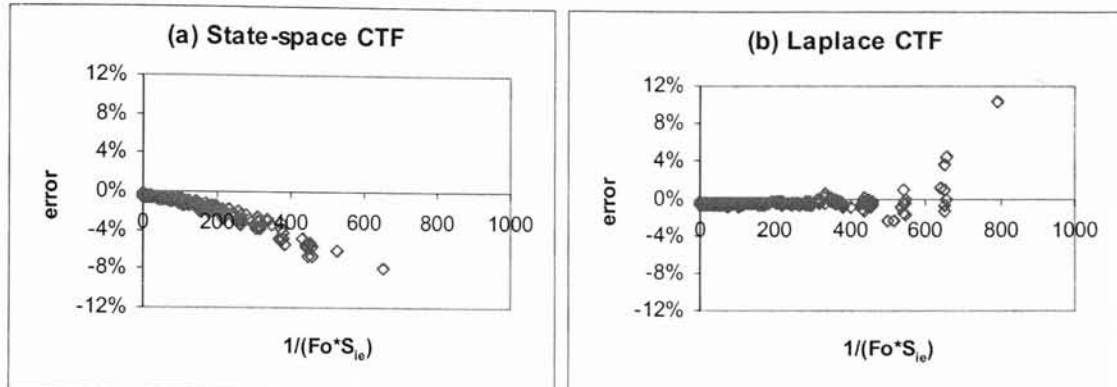


Figure 3.7 Single-layered CTF solution error (with thermal structure factor).

For the multi-layered cases, since the maximum number of layers is limited to 10 in the Toolkit algorithm, with the inner and outer layers are used to model the surface film resistances, the presented test procedure can only cover maximally 8 layers. Figures 3.8 and 3.9 show the CTF solution error for 3-layered and 6-layered slabs, respectively. The results are consistent with the single-layered case; as the material properties become thermally massive, the magnitude of error increases for the state-space CTF solution, and the error becomes increasing random for the Laplace CTF solution.

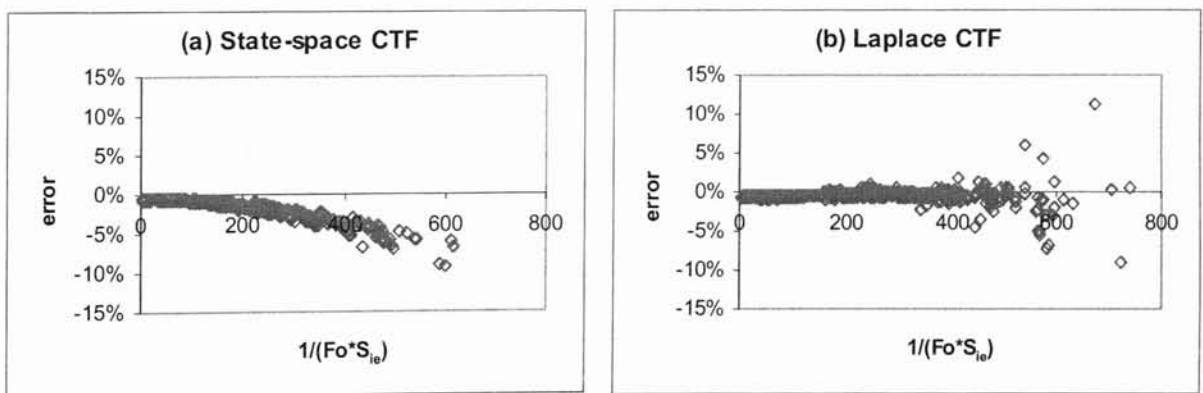


Figure 3.8 3-layered CTF solution error.



Note from figures 3.7, 3.8 and 3.9 that, as the number of layers increases, the state-space CTF solution error decreases for a specific value of  $1/(Fo \cdot S_{ie})$ . This correlation becomes obvious for heavy weight materials. Figure 3.10 shows the first values of  $1/(Fo \cdot S_{ie})$  that result in the state-space CTF solution errors bigger than 5%. The value of  $1/(Fo \cdot S_{ie})$ , i.e. the range of applicability is roughly constant for the state-space CTF solution in the entire range of number of layers. A slightly increase of  $1/(Fo \cdot S_{ie})$  is shown as the number of layers increases.

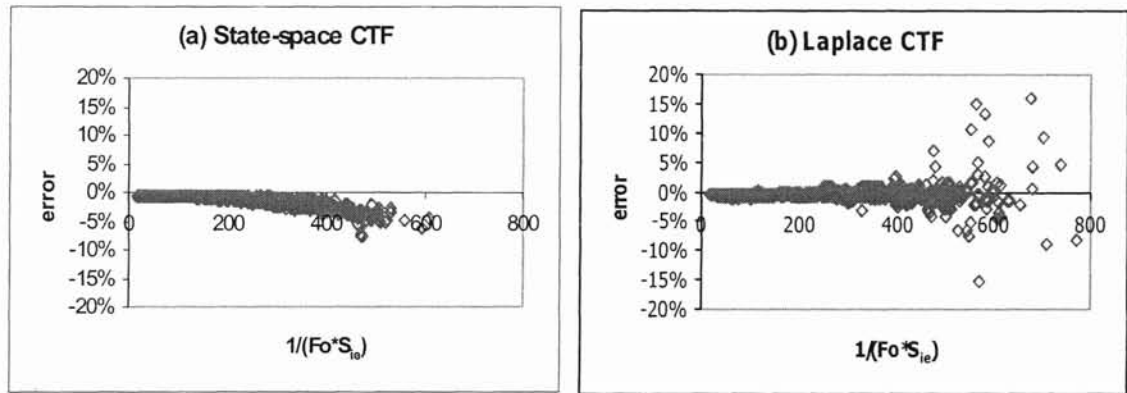


Figure 3.9 6-layered CTF solution error.

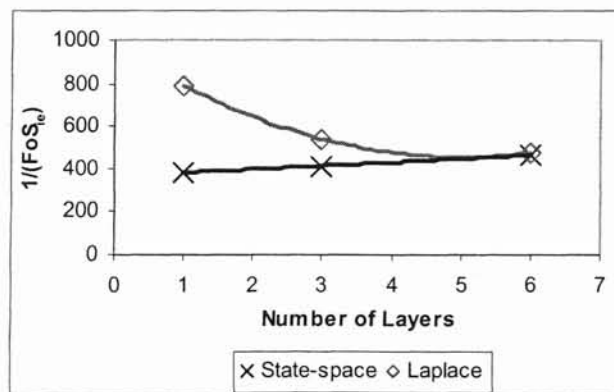


Figure 3.10 First values of  $1/(Fo \cdot S_{ie})$  that cause more than 5% error in the CTF solutions.

A similar curve can be also established for the Laplace CTF solution as shown in figure 3.10. Note that compared to the state-space CTF solution, an opposite trend is shown.

However, the value of  $1/(Fo \cdot S_{ie})$  changes rapidly with increasing number of layers.

Figure 3.10 shows that for small number of layers, the range of applicability is larger for the Laplace CTF than the state-space CTF. But as the number of layers is more than 6, the state-space CTF is expected to prevail over the Laplace CTF.

### 3.6 Conclusions

The conduction transfer function (CTF) is commonly used in transient conduction calculations. It is the numerical solution of the diffusion equation and Fourier's law. The test procedure presented in this chapter compared the ASHRAE Toolkit CTF solutions to the ASHRAE 1052-RP analytical solutions to benchmark the error in the CTF calculations and applications. The error sources are classified as CTF numerical error and application error as listed in table 3.1.

By changing material properties, the influence on the CTF solution errors was investigated for single- and multi-layered slabs. The CTF solution errors were plotted against the Fourier number and thermal structure factor such that the range of the errors can be approximated as shown in figures 3.4, and 3.7 to 3.9. Although the errors are relatively large for thermally massive constructions, the fluxes are typically very small. As a result, the impact on the cooling load is also small. For a 5% CTF solution error bound, figure 3.10 shows that the application range is roughly constant for the state-space CTF in the entire range of number of layers, while it is decreased for the Laplace CTF as the number of layers increases. The Laplace CTF shows a large application range than the state-space CTF for small number of layers.

## CHAPTER 4

### CALCULATING RADIANT TIME FACTORS FOR THE RADIANT TIME SERIES METHOD PROCEDURES

#### 4.1 Introduction

In addition to the periodic response factors (PRFs), the other set of predetermined coefficients used in the radiant time series method (RTSM) is the radiant time factors (RTFs). The RTFs are a time series that represents the time dependent thermal response of an adiabatic zone to a single steady periodic pulse of radiant energy incident on the zone internal surfaces. RTFs are a 24-coefficient series that is used to indicate the portion of the radiant pulse convected from the zone surfaces to the zone air at each hour. The RTSM uses the RTFs to determine the hourly contribution of the radiant heat gains to the cooling loads assuming that all heat gains entering into the building space must be eventually converted to cooling loads without any form of heat loss through the building envelope.

The RTFs are different for each unique zone geometry, construction, and radiation distribution. For a zone with the same construction on all surfaces, figure 4.1 illustrates the difference of RTFs for a light weight and a heavy weight zones subject to an identical unit radiant energy pulse. The relatively flat profile shown in figure 4.1a represents the slow thermal response of the heavy weight zone. The shape of the curve indicates a low heat extraction rate due to the strong thermal storage effect of the heavy weight materials. In addition, figure 4.1 also compares RTFs generated using different

radiation distributions. Typically, radiant heat gains are assumed to be either distributed only to the floor or distributed uniformly to all internal zone surfaces (Rees et al. 2000).

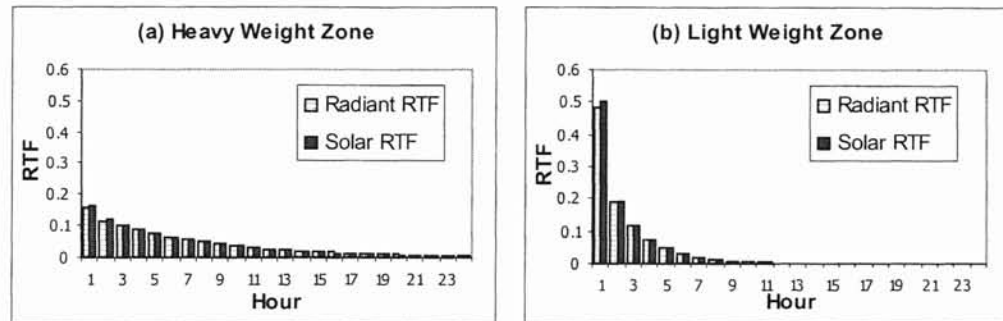


**Figure 4.1 Radiant Time Factors for different materials and radiant distributions.**

The beam RTFs shown in figure 4.1 take care of the solar distribution, while the diffuse RTFs take care of the uniform distribution. In the RTSM, the beam solar radiation is assumed to be incident only on the floor, while other sources of radiation (i.e. long wave radiation from internal gains or radiation exchange between internal surfaces, short wave radiation from lightings, diffuse solar radiation transmitted from windows, and the reflected diffuse radiation from the floor) are uniformly distributed to all zone surfaces. For purposes of calculating RTFs, the zone is considered adiabatic, regardless of differences in zone geometry, material properties and radiation distributions. This assumption ensures that no radiant energy leaves the zone during the RTF calculation. As a result, the summation of any unique RTFs is always equal to unity.

In addition, the heat gain conversion calculation in the RTSM can be simplified if the floor construction is similar to that of the other surfaces in the zone. As shown in figure 4.1, since all surfaces are constructed of the same material, the beam RTFs and diffuse RTFs are almost identical. As a result, a single set of RTFs would be enough to

convert all types of radiation heat gains to cooling loads. The validity of this simplification is discussed in section 4.4.

## **4.2 Using the Heat Balance Method to Calculate Radiant Time Factors**

The RTFs can be generated in two different ways. One is to derive the RTFs from weighting factors used in the Transfer Function Method (TFM). A number of weighting factors are available in the ASHRAE database (Spitler et al. 1997). However, the variety of the zone types and constructions is limited. Since the RTFs represent the thermal response of an adiabatic zone to a steady periodic radiant pulse, the other possible way to obtain RTFs is to model this process with the heat balance method (HBM). As long as the input radiant pulse is unity or the calculated hourly cooling loads are normalized with the input radiant pulse, the resulting 24-hour coefficients are the RTFs.

Figure 4.2 shows the procedures to calculate RTFs by means of the HBM. In order to calculate the desired RTFs, the zone geometry must be defined properly. This requires surface area and tilt angle for each zone surface. The construction information also needs to be specified in detail. Layer arrangements, long wave emissivity for all interior surfaces, and material properties for each layer are required as input parameters. The adiabatic zone boundary conditions make sure that no heat is transferred from the outside environment. This results in the thermal response of the zone to the radiant pulse alone. The HBM iterates for several days in order to converge on the steady periodic solution. To be consistent with the steady periodic assumption in the RTSM, the unit radiant heat gain is pulsed at the first hour on each calculation day. As shown in figure 4.2, only the radiation distribution differs in the calculation of solar and diffuse RTFs.

Depending on the radiation distribution, the resulting cooling loads from the HBM calculation are either beam RTFs or diffuse RTFs.

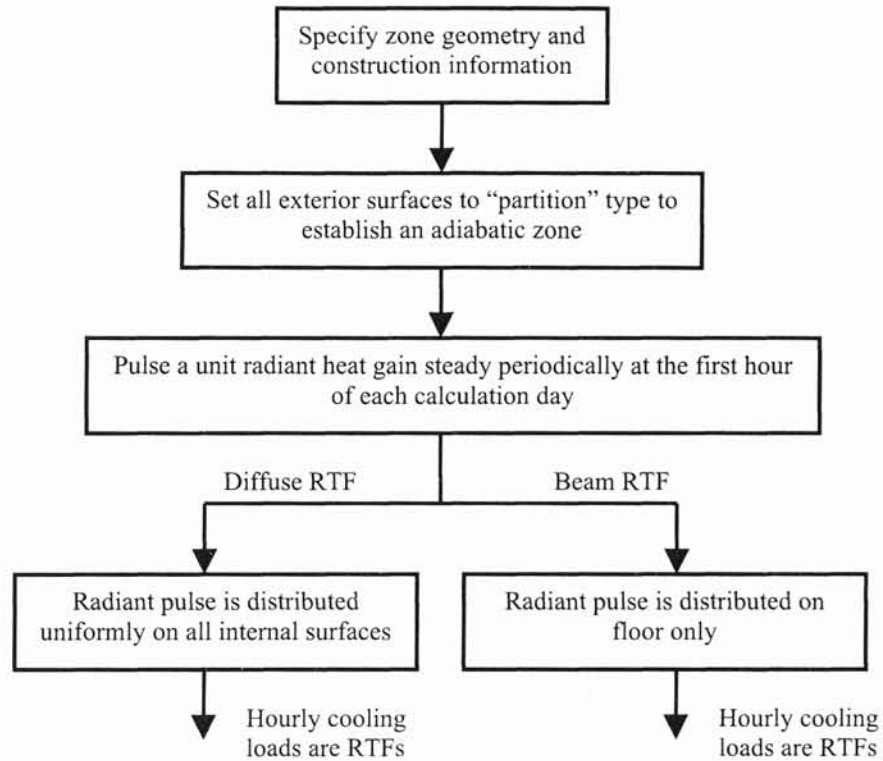
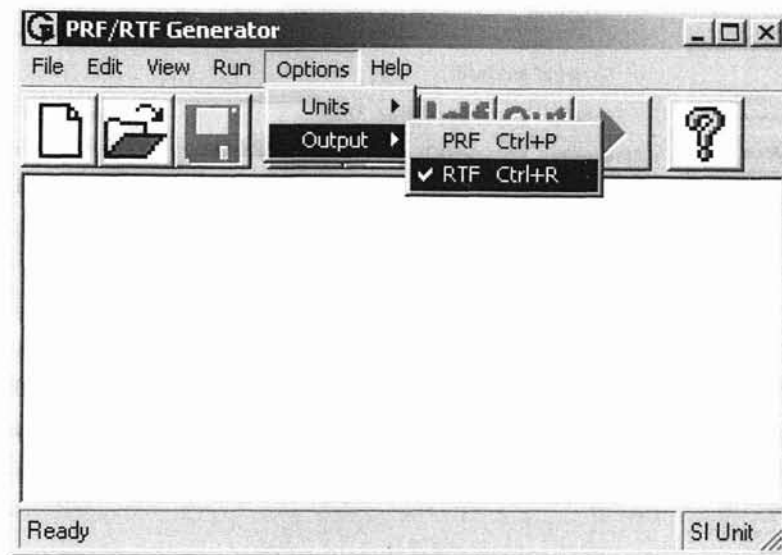


Figure 4.2 The RTF calculation procedures using HBM.

### 4.3 The Interface to the RTF Generator

The program described in chapter 2 was extended to include calculation of RTFs. Since the zone walls must be described in detail in order to calculate PRFs, very little additional information is required to calculate RTFs. In order to generate RTFs, the output option must be changed to "RTF" in the program as shown figure 4.3. The default output of the computer program is "PRF".



**Figure 4.3 Configure RTF calculations.**

Figure 4.4 shows the program interface of the RTF generator. The interface is identical to the PRF generator but with additional input parameters that are required for the RTF calculations. Note that the surface type options account for the tilt angle of the designated surface. The tilt angle is used as an indicator to the program to use an appropriate radiation distribution for the corresponding RTF calculation. For example, the floor is a horizontal surface with  $180^\circ$  tilt angle in the zone. The computer program is linked to a DLL file that calculates RTFs. The RTF calculation procedures were implemented with the Toolkit algorithms. Therefore, the program is capable of processing the Toolkit input files. Both solar and diffuse RTFs are calculated for any zone input.

**Surface Information**

Surface Number: 1 of 1

Surface Name: South Wall

Surface type:  Wall/Window  Floor  Roof/Ceiling  Internal Mass

Inside layer emissivity: 0.9 Area: 3 m<sup>2</sup>

No. of Layers: 5

Layer Name	Thickness mm	Conductivity W/(m·K)	Density kg/m <sup>3</sup>	Specific Heat kJ/(kg·K)	Resistance (m <sup>2</sup> ·K)/W	
1 F01					0.044	<input type="button" value="Edit"/>
2 M01	101.6	0.894	1922.153	0.795		<input type="button" value="Edit"/>
3 I02	50.8	0.029	42.448	1.214		<input type="button" value="Edit"/>
4 G01	15.875	0.16	800.897	1.088		<input type="button" value="Edit"/>
5 F02					0.12	<input type="button" value="Edit"/>

Note: Enter the outside layer first.  
Enter either thickness, conductivity, density, specific heat or resistance.  
For air-to-air PRF, outside and inside surface resistances should be input as the first and last layers respectively.

Figure 4.4 The computer program interface to generate RTFs.

#### 4.4 Evaluation of the Program Output

The RTF calculation procedure ensures that the unit radiant pulse must be entirely converted into cooling loads. The energy in the zone is always conserved and the resulting hourly cooling loads, (i.e. RTFs) must satisfy the following condition.

$$\sum_{j=0}^{23} r_j = 1 \quad (4.1)$$

Equation (4.1) is used to verify the program outputs. The sums of the RTF values calculated by the computer program for zones constructed of concrete, plywood, steel and insulation board are shown in table 4.1. Each construction is shown without windows and



with 50% glazing on two of the walls. The values of the corresponding zones with 50% glazing on two of the walls are also listed. The zone is 1×1×1 m (0.39×0.39×0.39 in) in dimension. The walls, floor and roof are all single-layered, 1.52 m (6 in) thick, and have the same material properties. The long wave emissivities for all inside surfaces are 0.9. Table 4.1 shows that the computational error in the generated RTFs is less than 0.5%. Note that because the RTFs are generated on the basis of an adiabatic zone, the addition of the highly conductive window doesn't significantly influence the accuracy of the RTF calculations.

**Table 4.1 Summations of 24-hour RTFs.**

Zone Types	Beam RTF		Diffuse RTF	
	Sum	Error	Sum	Error
HW Concrete	1.000005	0.0005%	1.000279	0.0279%
Plywood	1.000006	0.0006%	1.003728	0.3728%
Insulation Board	1.000018	0.0018%	1.004900	0.4900%
Steel	0.999899	0.0101%	0.999964	0.0036%
HW Concrete w/ Window	1.000032	0.0032%	1.000261	0.0261%
Plywood w/ Window	0.999999	0.0001%	1.003553	0.3553%
Insulation Board w/ Window	1.000013	0.0013%	1.004794	0.4794%
Steel w/ Window	0.999956	0.0044%	0.999976	0.0024%

Figures 4.5 to 4.8 show the hourly RTFs for the above zones. The high thermal capacity zones such as HW concrete and steel have slower thermal responses than the other zones. For the zones constructed with plywood and insulation board, a great portion of the heat gains absorbed by the surfaces are convected back to the zone air quickly in the early hours. Note that although the window construction doesn't influence the accuracy of RTFs, it alters the thermal response of the zones. This effect is more obvious for the diffuse RTFs of the high thermal capacity zones. Since the radiant pulse is assumed to be distributed uniformly on all internal surfaces, the portion of the heat gains distributed on the windows are quickly convected to zone air like they are for other low thermal capacity materials.

Since all zone surface constructions shown in figure 4.5a, 4.6a, 4.7a, and 4.8a are the same, either the solar or diffuse RTFs can be used to convert heat gains to cooling loads. Once one of the surface constructions is changed to a material of different thermal capacitance, figures 4.5b and 4.7b show that the two sets of RTFs are quite different. Even so, if the thermal capacitances of all the surface constructions are still comparable, a single set of RTFs can be used to simplify the problem as shown in figures 4.6b and 4.8b.

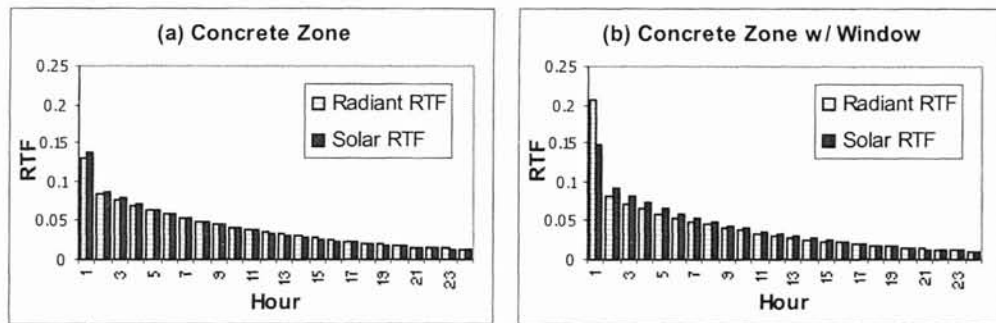


Figure 4.5 RTFs for concrete zones.

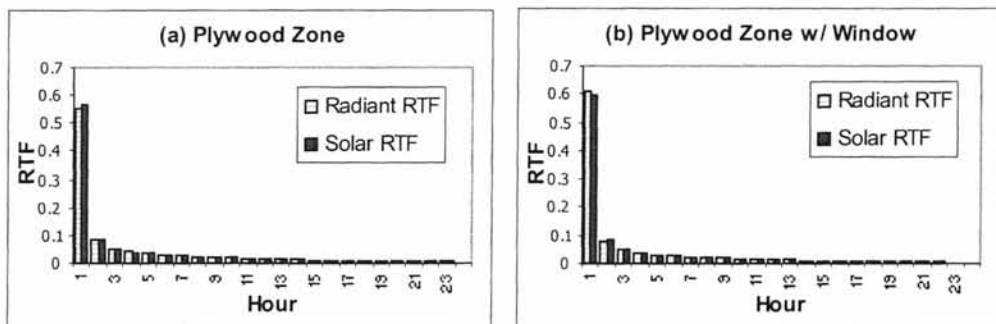


Figure 4.6 RTFs for plywood zones.

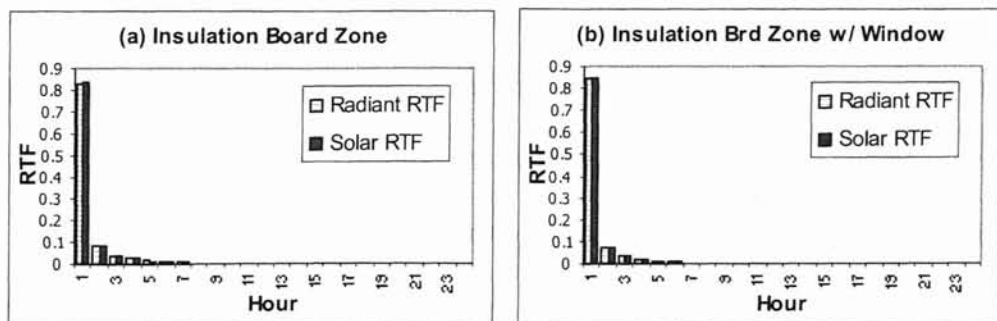


Figure 4.7 RTFs for steel zones.

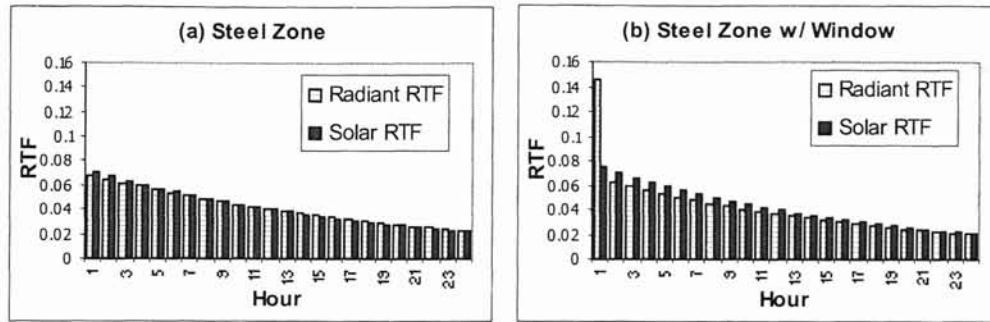


Figure 4.8 Insulation board zones.

#### 4.5 Using RTFs in the RTSM

The conversion of radiant heat gains to cooling loads in the RTSM is calculated by the following equation.

$$Q_{\theta} = r_0 q_{\theta} + r_1 q_{\theta-\delta} + r_2 q_{\theta-2\delta} + \dots + r_{23} q_{\theta-23\delta} \quad (4.2)$$

The hourly heat gains are operated on by each of the RTFs to approximate the instantaneous cooling load. Although the calculation is simple and straightforward, the use of RTFs introduces another source of error in the cooling load calculation. The calculation of RTFs is based on an adiabatic zone assumption that ignores the possibility of heat losses through the building envelope. As a result, the use of RTFs in the RTSM not only converts the radiant heat gains but also converts the heat losses into cooling loads. The heat losses include the reflected short wave radiation that is transmitted out through glazed surface and the radiative portion of conduction outflow due to adverse surface temperature gradients. Therefore, the cooling loads are always overpredicted in the RTSM. The validity of the adiabatic assumption is addressed in chapter 5 by means of an experimental evaluation.

## 4.6 Conclusions

The radiant time factors (RTFs) are used to convert radiant heat gains into cooling loads in the radiant time series method (RTSM). They represent the thermal response of a zone to a single steady periodic radiant pulse. There are two types of RTFs for a specific zone. The beam RTF is used to operate on the radiant heat gains that are only distributed on the floor, while the diffuse RTF is for other radiant heat gains that are uniformly distributed on all zone internal surfaces. If the thermal capacitance is similar for all zone surface constructions, a simple set of RTFs can be used for both beam and diffuse distributions. The conversion of radiant heat gains will be accurately approximated by a single set of RTFs.

RTFs can be calculated either from weighting factors or by using the heat balance method (HBM). This chapter described a detailed calculation procedure to generate RTFs using the ASHRAE Loads Toolkit heat balance method. An RTF calculation program using the ASHRAE Loads Toolkit algorithms was presented. The program outputs were evaluated for a particular zone with different materials. The resulting RTFs are satisfactory with an error less than 0.5%, and can correctly represent the corresponding thermal responses of different materials. Since an existing RTF database is not available, the computer program provides a convenient means to obtain RTFs for any particular zone geometry and construction. Although the program outputs are satisfactory, the use of RTFs in the RTSM overpredicts cooling loads, especially for zones with high radiant heat gains.

**CHAPTER 5**

**EXPERIMENTAL VERIFICATION OF THE RADIANT  
TIME SERIES METHOD FOR COOLING LOAD  
CALCULATIONS**

**5.1 Introduction**

In the previous chapters, two unique features of the radiant time series method (RTSM), PRFs and RTFs have been evaluated. In this chapter, the overall performance of the RTSM is investigated. The significance of errors due to conduction and radiation heat losses as well as the combined effect of other assumptions in the RTSM will be evaluated experimentally.

The RTSM is a simple cooling load calculation method provided that the periodic response factors and radiant time factors are known. However, the assumptions and simplifications built into the RTSM are possible sources of error in the cooling load calculations. Rees suggested that the ‘adiabatic zone assumption’, which is implicit in the generation of the radiant time series, coupled with the ‘air-to-air’ conduction calculation (Rees et al. 1998) is responsible for differences between the RTSM and the heat balance method. Applying the heat balance method to an adiabatic zone generates the radiant time series. Heat gains, once accounted for in the space, cannot be lost by either ‘surface-to-surface’ conduction or radiation from the space. Over-prediction of the cooling load occurs when radiation on the interior surfaces of the zone raise the inside surface temperature of a lightweight, resistive surface, such as a single pane of glazing, above the

outside surface temperature. In this case, two types of heat transfer immediately follow. First, the elevation of the inside surface temperature increases the rate of inside convection and, as a result, increases the cooling load. This phenomenon is modeled by the air-to-air conduction calculation in the RTSM. Second, the change in surface temperature could cause surface-to-surface conduction heat loss. As shown in figure 5.1, the sol-air to inside air temperature gradient ( $T_3-T_4$ ) is in the opposite direction of the inside surface to outside surface temperature gradient ( $T_1-T_2$ ). Under these conditions, the heat balance, which is based on the surface temperature gradient, predicts a heat loss while the RTSM, which is based on the air temperature gradient, predicts a heat gain.

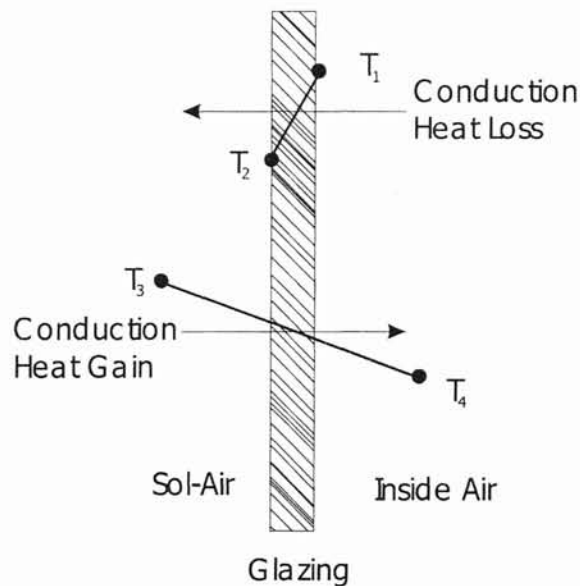


**Figure 5.1 Opposing Temperature Gradients Predicted by HBM and RTSM.**

Unaccounted for conduction losses occur during periods of high solar heat gains when interior surface temperatures rise to create a surface temperature gradient that is not predicted by the RTSM. Rees found that although the RTSM would never under-predict

the space loads, it could over-predict the peak cooling load by as much as 37% for cases with a high percentage of glazing and low internal heat gains.

Figure 5.2, which compares the heat balance and RTS methods, shows essential agreement between the methods for a lightweight zone with 90% glazing. The agreement was achieved by eliminating the two known sources of error discussed in the previous paragraphs. First, for purposes of illustration, the thermal resistance of the window was increased to eliminate conduction that the RTSM does not account for. Second, reflected solar radiation losses through the windows were calculated. These two modifications result in excellent agreement between the methods for all zone configurations. The reflected radiation correction, though not included in the ASHRAE Loads Toolkit, can easily be added to future versions of the method.

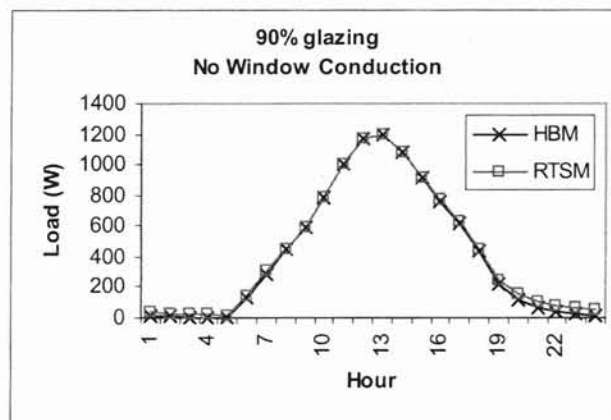


Figure 5.2 RTSM Modified to Correct Errors.

Some error may also be by assuming that surface convection and radiation coefficients are constant. This time invariant assumption, which is necessary for simplified PRF calculations, also influences the conduction heat gain split calculations as formulated in equation (1.1).

The objective of this investigation is to experimentally demonstrate the reliability of the RTSM as a simplified cooling load calculation procedure. This is accomplished by testing the extreme case of the solar dominated zone. Although the heat gain splits experimentally measured for this zone would not normally be encountered in most buildings (the solar heat gain exceeded 65% of the total heat gain for the test buildings), these conditions were selected in order to bound the error associated with RTSM procedure. For all zones with a smaller fraction of solar to total heat gain, the expected error due to the procedure is less. With these assumptions in mind, a test procedure was developed to investigate the sources of error in the RTSM. A “worst-case” scenario was used for the study—two buildings with highly glazed surfaces. The buildings, which are described in section 5.2.1 are designed to differentiate between massive and lightweight structures.

## **5.2 Validation Approach**

The RTSM validation was conducted by comparing cooling loads calculated using the RTSM to measured cooling loads. Using appropriate metrics, the validity of simplifying assumptions was analyzed, and the accuracy of heat transfer models was studied.

### 5.2.1 Facility Construction and Instrumentation

Two geometrically identical buildings, one thermally massive and one thermally lightweight as described by Eldridge et al. (2003), were constructed in an open field in



Stillwater, Oklahoma. The first floor of each building consists of a mechanical/control room that provides conditioned air to the test cell located directly above, as shown figure 5.3. The control room air temperature is maintained at the same temperature as the test cell in order to minimize heat conduction through the floor.

Elliptical flow nozzles measure the volumetric flow rate in the air loop. The room inlet and outlet air temperatures are also measured using thermocouple grids located in the ducts. The cooling load can then be calculated using the following equation.

$$Q_{\theta} = \dot{m}_{\theta} c_p (T_{out,\theta} - T_{in,\theta}) \tag{5.1}$$

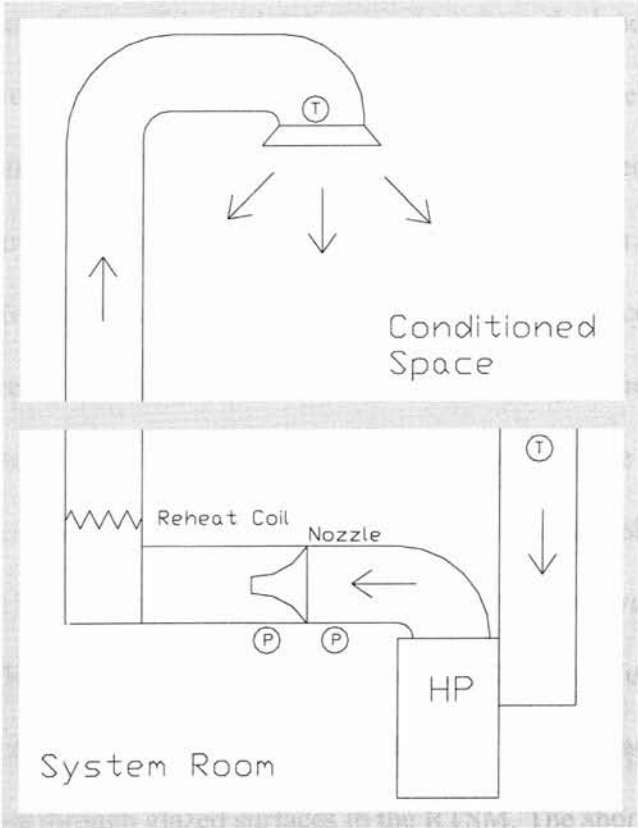


**Figure 5.3 Terminal reheat system used in the RTSM validation (not to scale).**

### 5.2.2 Validation Models

The measured cooling loads were compared to cooling loads predicted by three RTSM cooling load models, the baseline model, the tuned model and the modified model. All RTSM models were based on the ASHRAE Loads Toolkit (Pedersen, 2001) algorithms to develop.

- a) **Baseline Model Validation:** The baseline model uses simple Toolkit algorithms and estimated material properties and published weather data as input values. As such it provides an estimate of the uncertainty associated with the RTSM under typical field use conditions. The sources of error of this validation level are from the load calculation procedure and the uncertainties associated with estimating input parameters.
- b) **Tuned Model Validation:** The tuned model uses more sophisticated algorithms in the Toolkit, and uses measured input data in the calculation. It provides an estimate of the capability of the RTSM using measured input data. This validation procedure minimizes the error due to incorrectly estimated inputs. The measured input parameters are: outdoor and indoor temperatures, ground surface temperature, infiltration, globe horizontal solar radiation, wind speed, wind direction, system air flow rate and surface short wave absorptances. Table 5.1 shows how the measured data are used in this validation.
- c) **Modified Model Validation:** The modified model uses the same Toolkit algorithm and input data as that used in the tuned model. In addition, it is able to account for short wave radiation heat loss through glazed surfaces in the RTSM. The short wave radiation heat loss is due to short wave radiation from internal gains, diffuse solar radiation, and the portions of transmitted solar radiation heat gains that are reflected from the floor and transmitted out of the space through the windows.

The calculation procedure of the modified RTSM includes a model to determine the amount of short wave radiation heat gain that is transmitted out of the building space through the windows. The total diffuse short wave heat gain is calculated as:

$$q_{sw,\theta} = q_{r,beam,\theta} + q_{diffuse,\theta} + q_{sw,int,\theta} \quad (5.2)$$

where  $q_{r,beam}$  is the portion of the beam radiation that is reflected diffusely from the floor.

By assuming that the beam solar radiation is distributed only on the floor, while the diffuse solar radiation is distributed uniformly on each interior surface,  $q_{r,beam}$ , can be calculated as follows:

$$q_{r,beam,\theta} = s_{floor} \rho_{t,floor} q_{beam,\theta} \quad (5.3)$$

where  $s_{floor}$  is the solar fraction and  $\rho_{t,floor}$  is the short wave reflectance of the floor. Note that the values of  $q_{beam}$  and  $q_{diffuse}$  are available in the standard RTSM calculation procedures. The total diffuse short wave radiation heat loss through the windows is related to the total short wave heat gain in the zone as shown in equation (5.4).

$$q_{sw,loss,\theta} = q_{sw,\theta} \sum_{k=0}^{\#windows} s_k \tau_{t,k} \quad (5.4)$$

where  $s$  is the solar fraction and  $\tau_t$  is the transmittance of the windows. In the RTSM, the solar and radiant gains are operated on by RTFs to obtain cooling loads. In order to properly account for the loss of solar radiation that is reflected from interior surfaces and leaves the space through the windows, the short wave radiation heat loss must be calculated and subtracted from the hourly total radiant heat gain before the radiant heat gain is processed by the RTFs.

This single modification of the Toolkit RTSM algorithm, will correct the solar heat gain, but does not account for possible conduction losses from the zone.

Unaccounted for conduction losses occur during periods of high transmitted solar heat gains when high interior surface temperatures create an adverse temperature gradient that is not predicted by the RTSM. Since the RTSM relies on air-to-air PRFs to calculate the conduction heat gain, the method has no way of determining the effect of surface temperatures on the conduction process.

Modifications to the Toolkit were made in order to use the measured input parameters in the tuned and modified test suites. Table 5.1 summarizes the use of input parameters and the associated heat transfer models used in the RTSM. The measured parameters are the hourly input parameters in the associated Toolkit modules. In addition, in order to agree with the RTSM assumptions, average measured indoor temperatures are used in the calculation procedure. The PRFs and RTFs are generated using average outside and inside surface film coefficients.

Chantrasrisalai et al. (2003) addressed that the inside heat balance parameters have a major impact on the resulting cooling load. This is particularly true of the inside convection because it results in a direct contribution to the cooling load. Table 5.2 compares the ASHRAE natural convection coefficients to the ceiling-diffuser convection coefficients (Fisher et al. 1997) used in this validation. Note that the convection coefficients in the ASHRAE model are based on “reduced convection” at the ceiling due to thermal stratification. As a result the ASHRAE model under estimates the inside convection for the high ventilation rates present in the test buildings.

**Table 5.1 Summary of input parameters and heat transfer models for the RTSM validation.**

<b>Input Data / Heat transfer Models</b>	<b>Baseline Model</b>	<b>Tuned Model</b>	<b>Modified Model</b>
Indoor air temperature	Measured data	Measured data	Measured data
Sol-air temperature	<ul style="list-style-type: none"> <li>Simplified sol-air temperature model, equation (1.3)</li> <li>Long wave correction term</li> <li>Constant outside film coefficient.</li> <li>Measured outdoor air temperature</li> <li>Exterior surface SW absorptances: 0.9 for roofs, 0.5 for other surfaces</li> </ul>	<ul style="list-style-type: none"> <li>Detailed sol-air temperature model, equation (1.2)</li> <li>Measured outdoor air temperature</li> <li>Measured short wave absorptances: 0.9 for roofs, 0.7 for heavy building and 0.6 for light building exterior surfaces</li> <li>Measured ground surface temperature</li> <li>Blast sky temperature model</li> <li>ASHRAE surface view factor model</li> </ul>	<ul style="list-style-type: none"> <li>Detailed sol-air temperature model, equation (1.2)</li> <li>Measured outdoor air temperature</li> <li>Measured short wave absorptances: 0.9 for roofs, 0.7 for heavy building and 0.6 for light building exterior surfaces</li> <li>Measured ground surface temperature</li> <li>Blast sky temperature model</li> <li>ASHRAE surface view factor model</li> </ul>
Sky (solar) radiation	ASHRAE Clear Sky model	Modified ASHRAE Clear Sky model with measured global horizontal solar radiation	Modified ASHRAE Clear Sky model with measured global horizontal solar radiation
Ground surface temperature	BLAST model	Measured data	Measured data
Conduction	State-space conduction (Seem, 1987)	State-space conduction (Seem, 1987)	State-space conduction (Seem, 1987)
Surface convection coefficients	<ul style="list-style-type: none"> <li>Outside: MoWitt model with daily design wind speed and direction</li> <li>Inside: ASHRAE model</li> </ul>	<ul style="list-style-type: none"> <li>Outside: MoWitt model with hourly measured wind speed and direction</li> <li>Inside: Fisher et al. model (1997)</li> </ul>	<ul style="list-style-type: none"> <li>Outside: MoWitt model with hourly measured wind speed and direction</li> <li>Inside: Fisher et al. model (1997)</li> </ul>
Surface radiation coefficients	<ul style="list-style-type: none"> <li>Outside: Walton model (1983)</li> <li>Inside: Walton model (1980)</li> </ul>	<ul style="list-style-type: none"> <li>Outside: Walton model (1983)</li> <li>Inside: Walton model (1980)</li> </ul>	<ul style="list-style-type: none"> <li>Outside: Walton model (1983)</li> <li>Inside: Walton model (1980)</li> </ul>
Infiltration	BLAST model with 0.25 ACH hourly measured values	BLAST model with 0.25 ACH hourly measured values	BLAST model with 0.25 ACH hourly measured values
Conduction heat gain splits	Recommended Splits, table 1.1	Detailed splits, equation (1.1)	Detailed splits, equation (1.1)
Short wave correction calculation	No	No	Yes

**Table 5.2 Comparison of interior convection models.**

<b>Convection coefficients</b>	<b>ASHRAE</b>	<b>Fisher et al.*</b>
Ceiling	1.250	20.497
Wall	4.679	7.294
Floor	4.370	5.380

\* - Based on 19.5 ACH

### 5.2.3 Experimental Procedure

For each set of experiments, the two test cells described in section 5.2.1 were identically configured. Both test cells had the same interior room configuration and the indoor temperatures were controlled to the same value for each test. In addition, the test cells had been sealed before the cooling data were collected.

Four interior room parameters were varied during the tests as shown in table 5.3. Each parameter was designed to test the performance of different aspects of the RTSM algorithm. The suspended ceiling, blind, carpet and thermal mass tests provided the information on convection heat transfer, solar radiation, beam radiation distribution, and diffuse radiation distribution and thermal storage effect, respectively.

No internal gains were considered in the tests. Test conditions were maintained for more than 24 consecutive hours prior to data collection in order to allow the space to reach a steady-periodic state. Measurements were collected on clear days. Hourly cooling loads were measured and compared to the results of the RTSM baseline, tuned and modified models.

**Table 5.3 Test cell configurations.**

Test	1	2	3	4	5	6
<b>Suspended Ceiling:</b> 2'x4' lay-in ceiling below bar joists	No	Yes	No	No	No	Yes
<b>White Venetian Blinds</b>	No	No	Yes (45° slats)	No	No	Yes (Horizontal slats)
<b>Carpet</b>	No	No	No	Yes	Yes	Yes
<b>Thermal Mass:</b> office furniture including desks, tables, chairs, and bookshelves filled with books	No	No	No	No	Yes	Yes

#### 5.2.4 *Experimental Uncertainty*

The uncertainty in the cooling load measurement is related to equation (5.1), which can be also written as:

$$Q_{\theta} = \rho_{air} \dot{v}_{\theta} c_{p,air} (T_{out,\theta} - T_{in,\theta}) \quad (5.5)$$

where  $\dot{v}$  is the measured volumetric flow rate of air. According to the ASHRAE standard (1985), the uncertainty associated with this measurement is calculated as shown below:

$$e_{\dot{v}} = \pm \sqrt{e_c^2 + e_a^2 + e_{fs}^2 + e_{\Delta p}^2 + e_{sp}^2} \quad (5.6)$$

The typical uncertainties provided by the ASHRAE standard for the nozzle discharge coefficient and the nozzle area are:

$$e_c \pm 0.012$$

$$e_a \pm 0.005$$

The pressure transducer used in the measurement cannot measure pressure drop below 0.2 inches water, therefore the maximum fractional errors for the static and differential pressure are:

$$e_{sp} \pm 0.01$$

$$e_p \pm 0.01$$

The fan is accurate to provide constant speed  $\pm 1\%$ , i.e.  $e_{fs} = \pm 0.01$ . Therefore, the fractional uncertainty in the volumetric air flow measurement is:

$$e_v \pm 0.02$$

The uncertainties of the inlet and outlet temperature are estimated as:

$$T_{in} = \pm 0.5 \text{ } ^\circ\text{C}$$

$$T_{out} = \pm 0.5 \text{ } ^\circ\text{C}$$

Thus the uncertainty in terms of temperature difference is:

$$e_{\Delta T} = \sqrt{0.5^2 + 0.5^2} \approx \pm 0.71 \text{ } ^\circ\text{C}$$

Since the density and specific heat are calculated based on the measured temperature, the uncertainty associated with these variables is negligible. The uncertainty of cooling load is primarily due to the uncertainty associated with the volumetric flow rate and temperature difference. The fractional uncertainty of cooling load is therefore calculated as:

$$e_Q = \sqrt{e_v^2 + \left(\frac{e_{\Delta T}}{\Delta T}\right)^2}$$

or

$$e_Q = \sqrt{0.02^2 + \left(\frac{0.71}{\Delta T}\right)^2}$$



For a 10 °C temperature difference, the uncertainty of the measured cooling load would be about ±7.4%.

### 5.3 Results and Discussions

#### 5.3.1 Predicted Heat Gains

For a 40 C (104 F) design day outside dry bulb and constant 25 C (77 F) inside air boundary temperatures, table 5.4 shows the individual heat gain contribution to the total heat gain for the light weight building with the base configuration. The heat gain fractions were calculated from the following formulation:

$$q^* = \frac{\sum_{\theta=1}^{24} q_{\theta}}{\sum_{\theta=1}^{24} q_{tot,\theta}} \quad (5.7)$$

The fractions of infiltration, air-to-air conduction, transmitted solar and internal heat gains are shown in the table:

**Table 5.4 Typical Light Building Heat Gain Splits**

<b>Component Heat Gain</b>	$q^*_{infil}$	$q^*_{cond}$	$q^*_{solar}$	$q^*_{internal}$
<b>Heat gain fraction</b>	0.65%	31.85%	67.50%	0.0%

For the test building, the cooling load is dominated by the solar heat gain with a significant contribution from the conduction heat gain. Infiltration is insignificant, and internal gains are non-existent. Since the air-to-air conduction heat gain is calculated using the sol-air temperature and air-to-air PRFs, the conduction heat gain includes convection, long wave radiation and surface incident solar radiation in addition to

surface-to-surface conduction. As a result, the contribution of air-to-air conduction to the total heat gain is relatively high.

The heat gain splits shown in table 5.4 represent extreme operating conditions, and the procedural error associated with these conditions is significant. Rees calculated the deviation of the peak RTSM cooling load from the peak HBM cooling load for 1296 cases. Figure 5.4 shows the experimental test case data predicted by the modified RTSM superimposed on the Rees data.

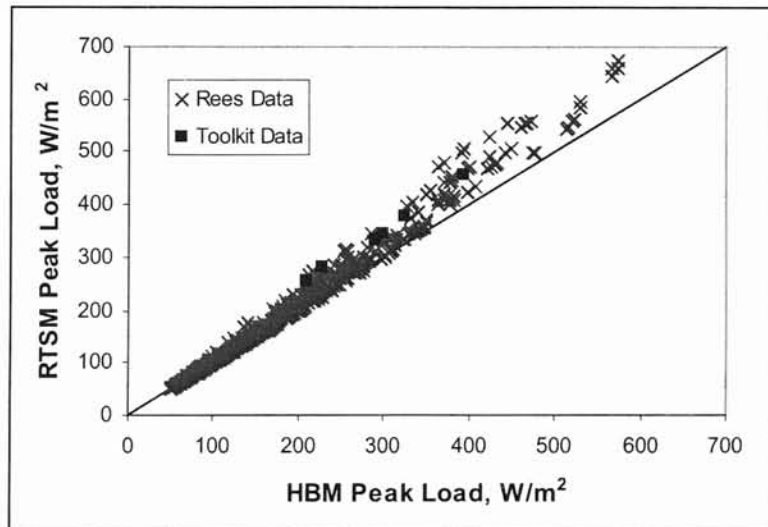


Figure 5.4 Comparison of Toolkit Results with Rees Parametric Study (Rees 2002).

As shown in the figure, the experimental test cases are well within the expected range of uncertainty for the RTSM even though they represent extreme operating conditions.

Figure 5.4 shows a deviation from the heat balance of less than 23% for all cases, even when the peak cooling load is relatively low. For cooling loads greater than 300 W/m<sup>2</sup> (95.13 Btu/hr-ft<sup>2</sup>) the modified RTSM deviates from the HBM by less than 17%.

### 5.3.2 Modeling of Thermal Mass Effect

The thermally massive test cell was constructed of eight-inch (20.32 cm), filled, heavyweight concrete block with a brick veneer, a five-inch (12.7 cm) concrete roof and a five-inch (12.7 cm) concrete floor. The lightweight test cell consisted of wood-framed walls with an exterior insulated finish system (EIFS) veneer, a built-up insulated roof and a 3.5-inch (8.89 cm) concrete floor. Both test cells had large windows (50% glazing) on the south and west walls. The periodic response factors shown in Figure 5.5 illustrate the different thermal responses of the building elements.

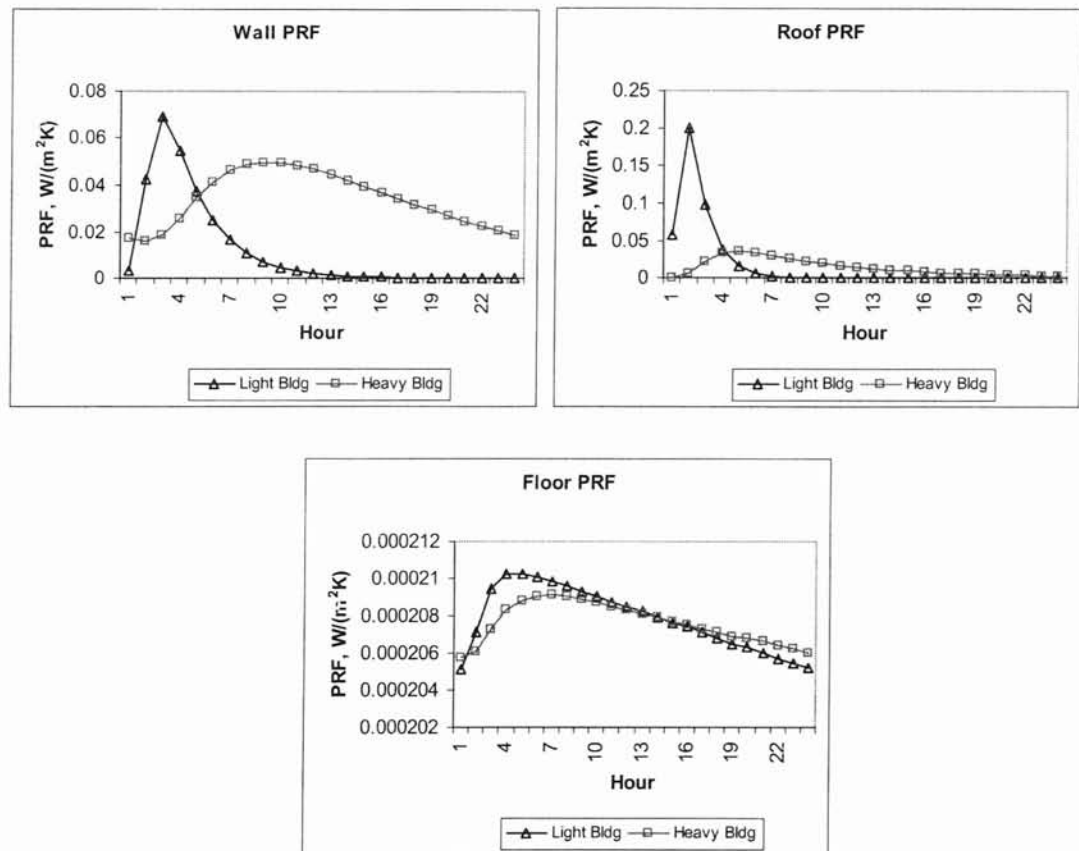


Figure 5.5 Periodic Response Factors for Test Buildings Surfaces.

The abrupt change of the wall and roof PRFs for the light building means that the thermal responses of these surfaces are faster than the heavy building wall and roof.

Based on the surface response factors, one might expect the zone thermal response to be significantly different for the two buildings. However, the dominance of the solar heat gain ensures that the RTFs rather than the PRFs will largely determine the zone response.

Figure 5.6 shows the radiant time factors for diffuse and beam solar radiation.

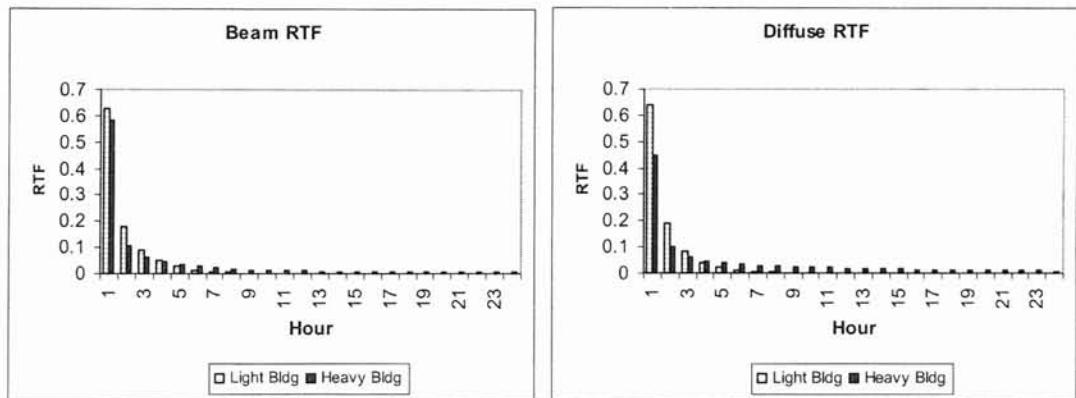
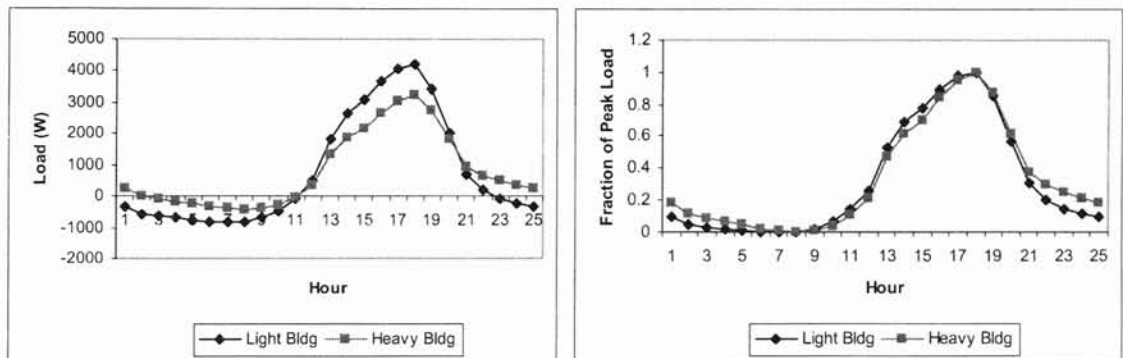


Figure 5.6 Radiant Time Factors for Test Buildings.

The difference between diffuse RTF and beam RTF is due to different radiation distributions. The diffuse RTF assumes that radiation is distributed uniformly on all interior surfaces, the fast thermal response of the light weight walls and roof causes the diffuse RTF to decrease faster. The beam RTF assumes that radiation is distributed only on the floor; and since the building floor constructions are similar, the zone RTFs are also similar. The overall effect of the building thermal mass is shown in Figure 5.7. The figure shows the measured cooling load for the two buildings under identical operating conditions. As shown by the ‘Load’ plot, the thermal mass of the heavy building damps the peak load by 25% but shows no discernible shift in the peak hour. The ‘Fraction of Peak Load’ plot shows the same cooling load profiles normalized as follows:

$$Q_N = \frac{Q_{est} - Q_{min,exp}}{Q_{max,exp} - Q_{min,exp}} \% \quad (5.8)$$

where  $Q_N$  is the normalized cooling load;  $Q_{est}$  is the estimated cooling load;  $Q_{min,exp}$  and  $Q_{max,exp}$  are the minimum and maximum measured cooling loads, respectively. Presenting the measured data in this way shows that the thermal response time of the two buildings are very similar in spite of significant differences in the building thermal mass.



**Figure 5.7 Thermal Mass Effects.**

As reported by Chantrasrisalai et al. (2003), the HBM correctly predicts both the peak load reduction and the peak time. The HBM models were therefore used in a small parametric study to gain additional insight into the thermal response of the experimental buildings. As a result of this simulation study, the following conclusions are reached:

- The high percentage of glazing on the south and west walls (50% by outside surface area) effectively “short-circuits” the building thermal mass. Removing the windows in the simulation study results in a significant time shift.
- The peak time is relatively insensitive to the magnitude of interior convection coefficient. High convection coefficients associated with 19.5 ACH and natural convection coefficients for both high glazing and no glazing cases result in less than a 0.5-hour change in the peak hour.

Although the convection coefficient has little effect on the peak time, it has a significant effect on the magnitude of the peak load. Chantrasrisalai et al. (2003) shows that significant error can be introduced in the peak load calculation by not adjusting the convection coefficients to match the ventilative flow rate required to meet the hourly cooling load. For example, using the ASHRAE default (natural convection) correlations to model the heavyweight buildings (which required 20 ACH to meeting the cooling load) results in under-prediction of the peak load by more than 20%.

### 5.3.3 Prediction of Peak Cooling Loads

Cooling load data for each of the test configurations were collected and compared with the RTSM predicted results as shown in figures 5.8 and 5.12 to 5.14. Each plot shows both measured and predicted hourly cooling loads which are defined in the figures as follows:

Measured – Measured cooling load

HBM – Cooling load predicted by heat balance method with measured input data

RTSM-Baseline – Cooling load predicted by the RTSM-Baseline model

RTSM-Tuned – Cooling load predicted by the RTSM-Tuned model

RTSM-Modified – Cooling load predicted by the RTSM-Modified model

All cooling loads are shown as a fraction of the measured load range. The actual load range (peak load and minimum load) used to calculate the fraction of full load is also shown in each figure. Showing the data as a fraction of measured load facilitates estimation of the peak load error associated with the RTSM and the HBM for each case. The peak error associated with each method can be read directly from the graphs.

### 5.3.3.1 Test 1: Base Configuration

Test 1 compares the measured cooling loads for an empty room with the RTSM predicted loads. The comparison is shown in figure 5.8. The difference between the RTSM-Baseline and tuned and modified models is a result of the different solar radiation, sol-air temperature, convection and conduction heat gain split algorithms used by the two models (Table 5.1). As expected, the tuned model results match the measured data better than the baseline model results. During the off-peak hours, conduction and convection are the dominant heat transfer processes in the space. The effect of using different convection algorithms in the models is apparent, as shown in the significant difference in cooling load.

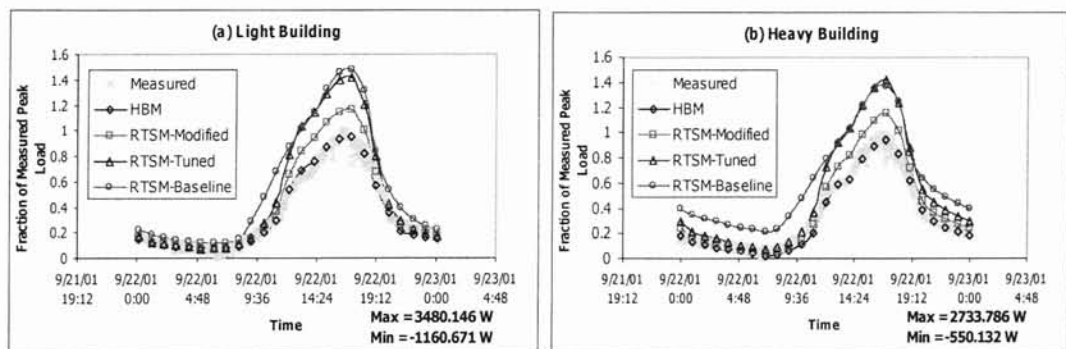


Figure 5.8 Test 1 - Base configuration.

Although most of the input uncertainties are eliminated in the tuned model, the RTSM still over predicts the peak cooling load. This is due to two uncorrected errors in the Toolkit RTSM. First the adiabatic zone is always assumed in the RTF calculation results in under prediction of the conduction heat loss as discussed in section 4.5. Second, solar radiation heat losses by transmission out of the space through the glazed surfaces are unaccounted for in the Toolkit algorithms. Although the conduction heat loss error is

not easily corrected in the Toolkit algorithms, the radiation correction as discussed in section 5.2.2 was included. The RTSM-Modified curves represent the RTSM-Tuned model with the short wave heat loss correction. As shown in figure 5.8, the correction can reduce the peak load errors in both buildings by about 50%.

In addition to the heat loss from short wave radiation and conduction, error is introduced in the RTSM by assuming that surface convection and radiation coefficients are constant. This time invariant assumption, which is necessary for simplified PRF calculations, also influences the conduction heat gain split calculations as formulated in equation (1.1).

The damping effect of the thermally massive heavy building is also shown in figure 5.8. The cooling load is shifted off peak by the heavy building resulting in a 25% reduction in the peak cooling load.

#### 5.3.3.2 Test 2: Suspended Ceiling

This test configuration required installation of suspended ceilings in the test cells, as shown in figure 5.9. Note that the diffuser remained fixed at the same level for both the suspended ceiling and the base case configuration. The correlation used to obtain the ceiling convection coefficient was a better match for the suspended ceiling case than for the base case. That is, the correlations were developed for an attached radial ceiling jet (Fisher et al., 1997). As a result, the error in the cooling load predicted by the RTSM was less for the suspended ceiling case as shown in figure 5.10. The basic trends, however, were the same with the radiation loss correction significantly improving the results, and the remaining peak errors about the same for the both buildings.



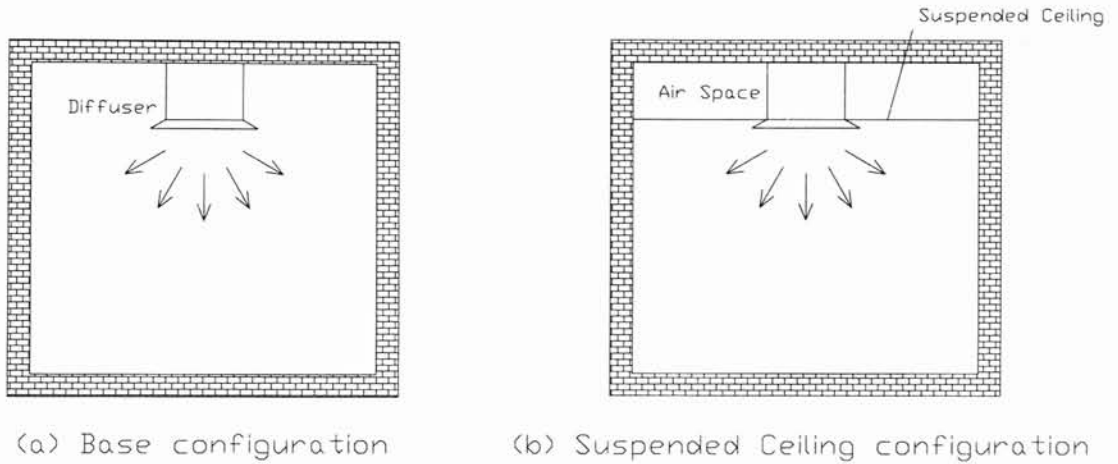


Figure 5.9 Test cell configurations.

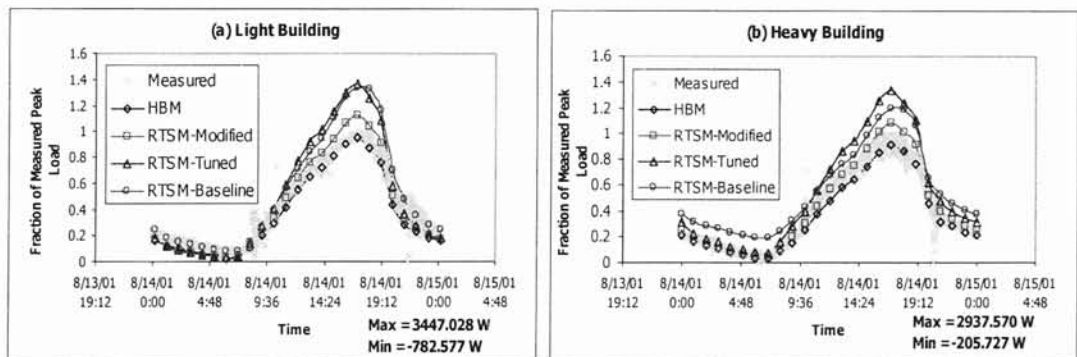


Figure 5.10 Test 2 - Suspended ceiling.

### 5.3.3.3 Test 3: Venetian blinds

The Venetian blind configuration is the same as the base configuration but with blinds mounted just inside the interior window surfaces. Figure 5.11 compares the hourly cooling load predicted by the various RTSM models. Note that since there are shades on the windows, a higher percentage of solar beam transmitted heat gain is blocked.

However, the diffuse solar heat gain could be higher than the previous cases because a portion of the transmitted beam radiation could be diffusely reflected into the

test cells. As a result, the reflected solar loss correction (RTSM-Modified) still showed a significant improvement over the other models. On the other hand, the blinds may influence the interior convection heat transfer coefficients on the window surfaces. This increases the uncertainty in the conduction calculation. The uncertainty of the shading coefficient also introduced error in the solar radiation calculation.

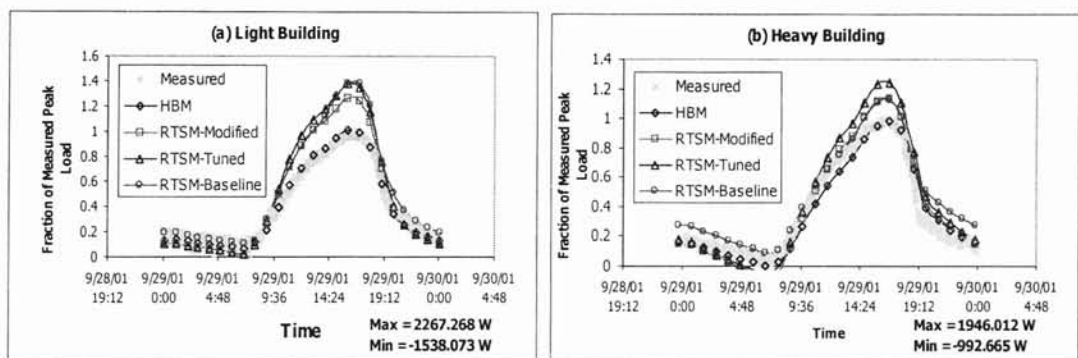


Figure 5.11 Test 3 - Blind with slats at 45°.

#### 5.3.3.4 Test 4: Carpet

Figure 5.12 shows the cooling load comparisons for the carpet configuration. The results are consistent with the previous cases showing that the RTSM results deviate from the heat balance results as expected. As shown in the figures, the HBM significantly overpredicts the peak load for the carpet cases. Discussions on these results can be found in the paper of Chantrasrisalai et al. (2003).

Although the RTSM over-predicts the heat balance load by less than 20%, it over-predicts the measured load by approximately 30%. This result illustrates the dependence of the RTSM on the heat balance procedure. Errors in the heat balance calculations are propagated to the RTSM through the radiant time factors and periodic response factors.

On the other hand, fundamental improvements in the heat balance parameters and algorithms will also be propagated to the RTSM resulting in overall improvement of the predicted cooling loads relative to the measured data.

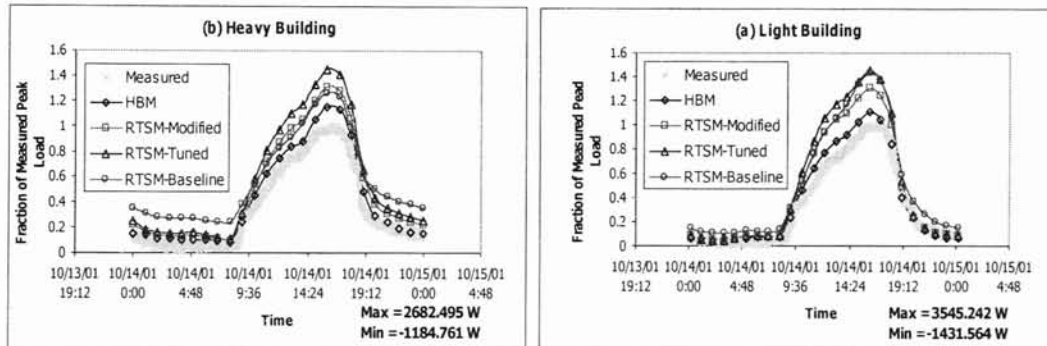


Figure 5.12 Test 4 – Carpet.

### 5.3.3.5 Test 5: Thermal Mass

The thermal mass configuration is the carpet configuration with some office furniture and books. The results shown in figure 5.13 are for the light building. Comparing these results to figure 5.12a, the RTSM-Modified model result is slightly more accurate for the thermal mass configuration. Since diffuse radiation is assumed to be distributed uniformly over all internal surfaces, the error reduction is due to the thermal mass shared portion of diffuse radiation heat gain, the amount of unaccounted for conduction loss from other surfaces is less than that of the carpet configuration. However, since solar radiation is the dominant heat gain in this zone, the increase of thermal mass cannot improve the RTSM results significantly.

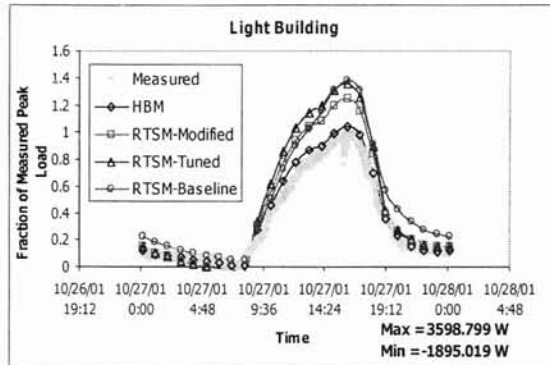


Figure 5.13 Test 5 –Thermal mass.

### 5.3.3.6 Test 6: Combined Configuration

Figure 5.14 shows cooling load comparisons for the combined configuration. This configuration includes, blinds, carpet and thermal mass. The blind slats are in a horizontal position resulting in higher beam solar radiation heat gains compared to the blind configuration. The blinds may also influence the surface convection coefficients in this test. The thermal mass in the test cells alleviates the unaccounted for conduction error and the suspended ceiling results in a better approximation of the interior convection coefficient at the ceiling level. The RTSM results behave consistently with the other configurations.

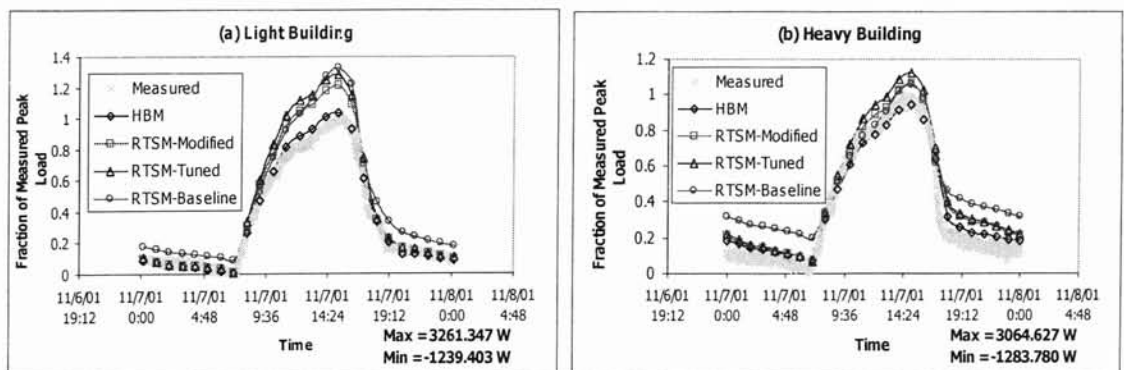
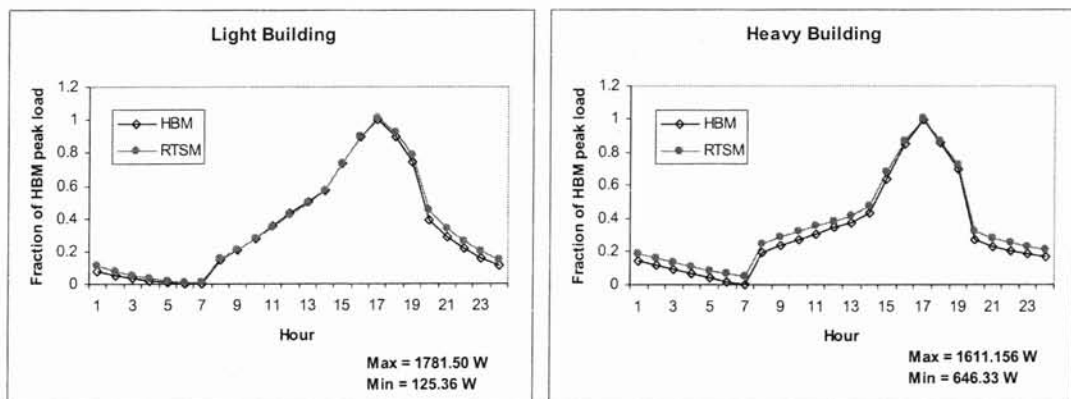


Figure 5.14 Test 6 - Combined configuration.

contribution of 67.5% of the total heat gain. For typical applications, the error is expected to be much less.

Figure 5.15 shows the office configuration calculated results for the test buildings modeled with a normal sized window [1.52-m by 1.52-m (5-ft by 5-ft)] on the west-facing wall. The window was changed in the model to a double-pane, low emissivity glass and is shaded all the time with a 45° Venetian blind. The boundary conditions are 40 C (104 F) design day outside dry bulb and constant 25 C (77 F) inside air temperatures. Internal heat gains were also considered in this simulation: two people are working in each building during office hours; two computers are used continuously and are in saver mode in the evening until the people come back the next morning; two 40 W lamps are on when the people are there.



**Figure 5.15 Simulations for typical building configurations.**

As shown in Figure 5.15, the RTSM results are almost identical to the HBM results. The off-peak load difference is due to the constant film coefficients used in the RTSM. Table 5.6 summarizes the individual heat gain contribution to the total cooling load for the light building. Comparing these heat gains to the experimental heat gains (table 5.4), table 5.6 shows that the air-to-air conduction heat gain dominates the thermal processes. Although

the window area is smaller, the transmitted solar heat gain still contributes significantly to the total cooling load. The internal heat gains are about 50% of the transmitted solar heat gains. The infiltration rate was not changed for the typical office simulation.

**Table 5.6 Heat gain fractions for typical building configurations.**

<b>Component Heat Gain</b>	$\dot{q}_{infil}$	$\dot{q}_{cond}$	$\dot{q}_{solar}$	$\dot{q}_{internal}$
<b>Heat gain fraction</b>	2.78%	55.81%	27.42%	13.99%

## 5.4 Conclusions and Recommendations

The experimental results illustrate the utility of the RTSM, even for the extreme case of a conditioned sunspace with no internal gains. As far as the peak load is concerned, although it has detailed input information, the tuned model does not show significant improvements over the baseline model. The modified RTSM over-predicts the heat balance by less than 20% for the well-defined zones. This is quite reasonable for the heat gain split (67.5% solar) observed in the experiments. Simulation of a typical building configuration with internal heat gains and less transmitted solar radiation, shows that the RTSM can be expected to match the HBM predicted peak cooling load for typical configurations.

The experimental results also highlight the importance of the reflected solar radiation correction for highly glazed zones. This correction can be easily implemented using information already available in the RTSM algorithms. It is recommended that the correction be included in the next version of the ASHRAE Loads Toolkit. Additional work to correct for the conduction losses from the zone is not recommended. The adiabatic zone assumption is an implicit simplification in the RTSM; derivation of

additional correction factors unnecessarily complicates the method. Rather, future research should be aimed at improving the heat balance models and refining and cataloging model input parameters. Improvements in the HBM will be propagated to the RTSM and result in the improved accuracy of both methods.

The research also illustrated the importance of choosing interior convection heat transfer coefficients on the basis of the ventilative flow rate. Using natural convection based correlations for high ventilative flow rates can result in significant error in the calculated cooling load. Finally, the dominant effect of windows in determining the peak hour for the experimental buildings was illustrated by the research results. The 50% glazing on west and south walls completely eliminated any peak hour shift between the heavy and light buildings. Additional research is required to determine the effect of advanced glazing systems on the peak cooling load.

## CHAPTER 6

### CONCLUSIONS AND RECOMMENDATIONS

#### 6.1 Conclusions

This thesis discussed the implementation and validation of the radiant time series method (RTSM) for cooling load calculations. The RTSM uses periodic response factors (PRFs) and radiant time factors (RTFs) to simplify the cooling load calculation procedures. PRFs represent the thermal response of a wall to a single steady periodic temperature pulse. Using PRFs with sol-air temperatures, the transient conduction problem is simplified such that conduction heat flux can be directly related to temperatures only. Similar to PRFs, RTFs represent the thermal response of a zone to a single steady periodic radiant pulse. In the RTSM, heat gains are split into convective and radiative components. The convective heat gains are directly contributed to the instantaneous cooling loads, while the energy storage and release effects of the radiative heat gains are operated on by the RTFs to become cooling loads. Both PRFs and RTFs are predetermined coefficients in the RTSM.

A calculation procedure to derive PRFs from conduction transfer functions (CTFs) is described in chapter 2, where the “air-to-air” and “surface-to-surface” CTFs/PRFs were clarified in terms of their physical meanings and applications. The procedures of using the ASHRAE Loads Toolkit modules to calculate CTFs and PRFs were discussed. A computer program using the Toolkit Modules was presented to



effectively calculate CTFs and PRFs for any constructions. The program outputs were evaluated based on:

1. Physical significance of the CTFs and PRFs.
2. Comparison to the published data.
3. Steady state accuracy.

The results showed that the outputs are satisfactory. An uncertainty analysis using the computer program showed that for a test case with 3.4% error in U-value resulted in less than a 1.5% error in the cooling load.

In addition to the calculation of the CTFs/PRFs, the application range of the Toolkit CTFs (state-space and Laplace) was investigated in chapter 3. The range of applicability is measured with Fourier number and thermal structure factor in the form of  $1/(FoS_{ie})$  to quantify the CTF solution error in conduction calculations. The higher value of  $1/(FoS_{ie})$ , the larger application range of CTFs is. For a 5% error bound, the state-space CTF shows a relatively constant application range ( $1/(FoS_{ie}) \approx 450$ ) for the entire range of the number of layers, while the application range for the Laplace CTFs decreases as the number of layers increases ( $1/(FoS_{ie}) \approx 800$  for single-layered slabs). The sources of the CTF solution error were due to the CTF calculation and CTF application. The investigation showed that the CTF solution errors are larger for the thermally massive constructions because of the small amount of conduction heat fluxes. As a result, the impact on the resulting cooling load is small.

A heat balance based calculation procedure to calculate RTFs is described in chapter 4. The difference between beam and diffuser RTFs was discussed. Since existing RTF data are not available in the literature. A computer program using the Toolkit

Modules was presented to conveniently calculate RTFs for any particular zone geometry and construction. The program outputs were evaluated in terms of the physical significance of the RTFs. The results are satisfactory with an error less than 0.5%. The results also showed that the beam and diffuse RTFs are approximately the same if the thermal capacitances of all building envelope elements are similar. The use of RTFs in the RTSM was also discussed in the chapter. Since RTFs are calculated based on an adiabatic zone assumption, the use of RTFs in the RTSM results in overprediction of cooling loads, especially for zones with high radiant heat gains.

The experimentally validation results of the RTSM were reported in chapter 5. To investigate the error due to the 'adiabatic zone assumption' used in the RTSM, cooling load data were collected from a heavy weight and a light weight test cells that are constructed with highly glazed surface area. Using the ASHRAE Loads Toolkit algorithm, the RTSM was validated in three versions: baseline, tuned and modified. The baseline model is based on minimum number of input parameters, and use simplified heat transfer models to run the RTSM. The tuned model uses detailed input data and sophisticated models in the cooling load estimation. Based on the same input data and heat transfer models of the tuned models, the modified model was developed to correct the possible radiation heat loss from windows. The RTSM validation was conducted by comparing predicted cooling loads to the measured data for different test cell configurations. The validation results showed that all the RTSM versions overpredicted the peak cooling loads for all the test cases. The baseline and tuned models predicted similar peak load errors. The modified model effectively reduces the peak load errors predicted by other models. For a well-defined zone configuration, the modified model

overpredicted the peak cooling load by 12.66%, while the tuned model overpredicted the peak cooling load by as much as 36.98%. Other possible sources of error of the modified model come from the unaccounted for conduction heat loss through the building envelope and the constant film coefficients used in the RTSM. Errors are also propagated from the heat balance method (HBM). The validation results also showed that the dominant amount of solar radiation heat gains through the windows completely eliminated the phase hour shift between the buildings. The magnitude of the interior convection coefficient although does not apparently influence the peak time, it has a significant effect on the magnitude of the peak load.

## 6.2 Recommendations

As a result of this investigation, the followings are suggested regarding the accuracy of the RTSM in cooling load calculations:

- For a 5% CTF error bound, the Laplace CTFs are recommended to use if the number of layers of a building fabric is less than 6. The application range of the Laplace CTFs changes from  $1/(FoS_{ie}) \approx 800$  for single-layered slabs to  $1/(FoS_{ie}) \approx 450$  for 6-layered slabs. The state-space CTFs are recommended if the number of layers is more than 6. The application range of the state-space CTFs is at  $1/(FoS_{ie}) \approx 450$  for the entire range of the number of layers in the Toolkit algorithm.
- In case of a building with similar thermal capacitances on all surfaces, a single set of RTFs is enough to convert all kinds of radiation heat gains into cooling loads.

As a result, the RTSM calculation procedures can be further simplified but without loss of accuracy.

- Since the short wave radiation correction on the adiabatic zone assumption significantly improves the RTSM on peak load estimations. It is recommended to include the short wave radiation correction in the future version of the RTSM.
- Although short wave radiation heat loss can be corrected, it is still not recommended to apply RTSM on buildings with highly conductive surface area due to the unaccounted for conduction heat loss in the RTSM.
- To preserve the simplified calculation procedures of the RTSM, additional work on the correction of the conduction heat loss through the building envelope is not recommended. Rather, future research should be focused on improving the heat balance models. Since the errors of the HBM are propagated to the RTSM, improvement in the HBM will also improve the RTSM accuracy.

## REFERENCES

- ASHRAE (1967). *ASHRAE Handbook of fundamentals*. Atlanta, GA: American Society of Heating, Refrigerating and Air-Conditioning Engineers, Inc.
- ASHRAE (1972). *ASHRAE Handbook of fundamentals*. Atlanta, GA: American Society of Heating, Refrigerating and Air-Conditioning Engineers, Inc.
- ASHRAE (1977). *ASHRAE Handbook of fundamentals*. Atlanta, GA: American Society of Heating, Refrigerating and Air-Conditioning Engineers, Inc.
- ASHRAE (1985). *ASHRAE Standard 51*. Atlanta, GA: American Society of Heating, Refrigerating and Air-Conditioning Engineers, Inc.
- ASHRAE (1997). *ASHRAE Handbook of fundamentals*. Atlanta, GA: American Society of Heating, Refrigerating and Air-Conditioning Engineers, Inc.
- ASHRAE (2001). *ASHRAE Handbook of fundamentals*. Atlanta, GA: American Society of Heating, Refrigerating and Air-Conditioning Engineers, Inc.
- Chantrasrisalai, C and D.E. Fisher (2003) *Experimental Verification of Design Cooling Load Procedures: Model Comparison*. To be published in ASHRAE Transactions.
- Chantrasrisalai, C and D.E. Fisher, Iu, I.S. and D. Eldridge (2003). *Experimental Verification of Design Cooling Load Procedures: The Heat Balance Method*. To be published in ASHRAE Transactions.
- Giaconia, C., and Orioli, A. (2000). *On the reliability of ASHRAE conduction transfer function coefficients of walls*. Applied thermal engineering, 20, 21-47.
- Ceylan, H.T. and Myers, G.E. (1980). *Long-time solutions to heat conduction transients with time-dependent inputs*. ASME Journal of Heat Transfer 102 (1), 115-120.

- Crawley, D.B., Lawrie, L.K., Pedersen, C.O., Liesen, R.J., Fisher, D.E., Winkelmann, F.C. and Buhl, W.F. (1998). *EnergyPlus: The New Generation Energy Simulation Program Beyond BLAST and DOE-2*. ASES Passive Conference, Albuquerque, New Mexico, Boulder, Colorado: ASES.
- Eldridge, D. and D.E. Fisher, I.S. Iu, C. Chantrasrisalai, 2003, *Experimental Validation of Design Cooling Load Procedures: Facility Design*, to be published in ASHRAE Transactions.
- Fisher, D.E. and Pedersen, C.O. (1997). *Convective Heat Transfer in Building Energy and Thermal Load Calculations*, ASHRAE transactions, 103 (2), pp. 137-148.
- Harris, S.M. and McQuiston, F.C. (1988). *A study to categorize walls and roofs on the basis of thermal response*. ASHRAE Transactions 94 (2): 688-715.
- Hittle, D.C. (1979). *Calculating building heating and cooling loads using the frequency response of multilayered slabs*, Ph.D. Thesis, University of Illinois at Urbana-Champaign.
- Incropera, F.P. and DeWitt, D.P. (1996). *Introduction to heat transfer*, 3rd ed. Wiley, New York, NY.
- Kossecka, E. (1998). *Relationships between structure factors, response factors, and Z-transfer function coefficients for multilayer walls*. AHSRAE transactions 104 (1A), 68-77.
- Loudon, A.G. (1968). *Summertime temperatures in buildings without air conditioning*. Building Research Station, Current Paper 47/68.
- McQuiston, F.C. and Spitler, J.D. (1992). *Cooling and Heating Load Calculation Manual, 2<sup>th</sup> Ed*. ASHRAE: 2.1-2.14.

- McQuiston, F. C., Parker, J. D. and Spitler, J.D. (2000). *Heating, ventilating, and air conditioning – analysis and design, 4<sup>th</sup> Ed.* New York, NY: John Wiley & Sons, Inc.
- Mitalas, G.P. (1978). *Comments on the Z-transfer function method for calculating heat transfer in buildings.* ASHRAE transactions 84.
- Ouyang, K. and Haghghat, F. (1991). *A procedure for calculating thermal response factors of multi-layered walls—state space method.* Building and Environment 26 (2), 173-177.
- Peavy, B.A. (1978). *A note on response factors and conduction transfer functions.* ASHRAE transactions 84.
- Pedersen, C.O. (2001). *Building loads calculation toolkit.* Atlanta, GA: American Society of Heating, Refrigerating and Air-Conditioning Engineers, Inc.
- Pedersen, C.O., Fisher, D.E. and R.J. Liesen (1997). *Development of a heat balance procedure for calculating cooling loads.* ASHRAE transactions 103 (2): 459-468
- Rees, S.J. (2002). Personal communication.
- Rees, S.J., Spitler, J.D., Davies, M.G. and Haves, P. (2000). *Qualitative comparison of North American and U.K. cooling load calculation methods.* International Journal of HVAC&R Research, ASHRAE 6 (1): 75-99.
- Rees, S.J., Spitler, J.D. and Haves, P. (1998). *Quantitative comparison of North American and U.K. cooling load calculation procedures – results.* ASHRAE transactions 104 (2): 36-46
- Seem, J.E. (1987). *Modeling of heat transfer in buildings, Ph.D. Thesis.* Madison, WI: University of Wisconsin-Madison.

- Seem, J.E. et al. (1989). *Transfer functions for efficient calculation of multidimensional transient heat transfer*. Journal of heat transfer 111, 5-12.
- Spitler, J.D. and Fisher, D.E. (1999). *On the relationship between the radiant time series and transfer function methods for design cooling load calculations*. International Journal of Heating, Ventilating, Air-Conditioning and Refrigerating Research 5 (2), 125-138.
- Spitler, J.D. and Fisher, D.E. (2000). *Development of periodic response factors for use with the radiant time series method*. ASHRAE Transactions
- Spitler, J.D., Fisher, D.E. and Pedersen, C.O. (1997). *The radiant time series cooling load calculation procedure*. ASHRAE Transactions 103 (2), 503-515.
- Spitler, J.D., Rees, S.J. and Xiao, D. (2001). *Development of an analytical verification test suite for whole building energy simulation programs – building fabric*. ASHRAE 1052-RP final report. Atlanta, GA: American Society of Heating, Refrigerating and Air-Conditioning Engineers, Inc.
- Stephenson, D.G. and Mitalas, G.P. (1971). *Calculation of heat conduction transfer functions for multiplayer slabs*. ASHRAE Transactions 77 (2):1.17.
- Walton, G.N. (1980). *A New Algorithm for Radiant Interchange in Room Loads Calculations*, ASHRAE transactions, Vol. 86, Part 2., pp. 190-208.
- Walton, G. N. (1983). *Thermal Analysis Research Program Reference Manual*. National Bureau of Standards. NBSSIR 83-265



VITA 2

IP SENG IU

Candidate for the Degree of

Master of Science

Thesis: EXPERIMENTAL VALIDATION OF THE RADIANT TIME SERIES  
METHOD FOR COOLING LOAD CALCULATIONS

Major Field: Mechanical Engineering

Biographical:

Education: Received Bachelor of Science degree in Electromechanical Engineering from the University of Macau, Macau in June 1999. Completed the requirements for the Master of Science degree with a major in Mechanical Engineering at Oklahoma State University in (December, 2002)

Experience: Employed by Department of Forestry, Oklahoma State University as a graduate research assistant, summer 2001; Employed by Department of Mechanical Engineering, Oklahoma State University as a graduate research assistant, 2000 to present.

Professional Memberships: Institute of Electrical and Electronics Engineers (IEEE), 1998 to 1999  
American society of Heating, Refrigerating and Air-Conditioning Engineers (ASHRAE), 2000 to present